

DEPARTMENT OF PHYSICS AND ASTRONOMY  
UNIVERSITY OF HEIDELBERG

Bachelor Thesis in Physics  
submitted by

**Manuel Jahn**

born in Kassel (Germany)

**2017**



# Quality assurance for gas electron multipliers with the leakage current test

This Bachelor Thesis has been carried out by Manuel Jahn at the  
Physikalisches Institut Heidelberg  
under the supervision of  
Priv.-Doz. Dr. Silvia Masciocchi



## **Abstract**

The implementation of Gas Electron Multipliers (GEMs) in the readout chambers of the Time Projection Chamber is a major part of the upgrade of the ALICE experiment. GEMs are perforated copper-clad Kapton foils that have electron multiplication abilities. A central quality measure for GEMs is the amount of leakage current under the application of a high voltage difference between the two copper layers. The measurement of leakage currents is the subject of this thesis. The measurement procedure is carefully described and various measurements are conducted aiming at the identification of the determining factors for the leakage current. A dependence on the GEM area and on the pitch size is found; larger area and smaller pitch size involve higher leakage current. Another examined factor, the storage air humidity, cannot unambiguously be related to the leakage current. Further, the measurement's reproducibility is found to be limited by undetermined sources of noise. By comparison with other institutes' measurement data, an estimate for the amount of noise is provided and possible causes are delineated.

## **Zusammenfassung**

Die Verwendung von Gas Electron Multipliers (GEMs) in der Time Projection Chamber ist ein bedeutender Teil der Aufrüstung des ALICE-Experiments. GEMs sind perforierte, zweiseitig mit Kupfer beschichtete Kapton-Folien, die zur Elektronenvervielfachung eingesetzt werden. Ein zentrales Qualitätsmaß für GEMs ist die Höhe des Leckstroms, der beim Anlegen einer Hochspannung zwischen den Kupferschichten fließt. Der Meßprozess ist der Schwerpunkt dieser Arbeit. Die Meßprozedur wird detailliert beschrieben und es wird eine Reihe von Messungen durchgeführt, die auf die Identifikation der bestimmenden Faktoren des Leckstroms zielen. Eine Abhängigkeit des Leckstroms von der Fläche und dem Lochabstand der GEMs wird festgestellt; der Leckstrom vergrößert sich mit steigender Fläche und sinkendem Lochabstand. Ein weiterer betrachteter Faktor, die Luftfeuchtigkeit bei der Lagerung, kann nicht eindeutig mit dem Leckstrom in Verbindung gebracht werden. Es wird weiterhin beobachtet, dass die Reproduzierbarkeit der Messungen durch unbekannte Störquellen eingeschränkt wird. Durch Vergleich mit den Messdaten eines anderen Instituts wird eine Abschätzung für die Höhe der Störung gefunden und letztlich werden mögliche Ursachen beschrieben.



# Contents

<b>1</b>	<b>Introduction</b>	<b>3</b>
1.1	A glimpse into the first moments after the Big Bang . . . . .	3
1.2	The ALICE experiment . . . . .	4
1.3	The Time Projection Chamber . . . . .	5
1.4	The Time Projection Chamber Upgrade . . . . .	8
<b>2</b>	<b>Introduction to Gas Electron Multipliers</b>	<b>10</b>
2.1	General approach to Gas Electron Multipliers . . . . .	10
2.2	The TPCU GEM design . . . . .	11
2.3	Main steps for quality assurance and the GEM production chain . . . . .	13
<b>3</b>	<b>GEM handling processes at GSI</b>	<b>14</b>
3.1	General GEM safety tips . . . . .	14
3.2	The leakage current measurement . . . . .	14
3.2.1	Testing equipment . . . . .	14
3.2.2	The test setup . . . . .	17
3.2.3	The testing procedure manual . . . . .	18
3.3	The framing procedure . . . . .	20
3.3.1	Framing equipment . . . . .	20
3.3.2	The framing procedure manual . . . . .	23
<b>4</b>	<b>Analytical approach to the leakage current test</b>	<b>25</b>
4.1	Leakage current measurement results . . . . .	25
4.2	The area dependence of the leakage current . . . . .	27
4.3	The pitch size dependence of the leakage current . . . . .	31
4.4	The foil humidity dependence of the leakage current . . . . .	33
4.5	Reproducibility of measurements . . . . .	36
4.6	Data comparison with other institutes . . . . .	39
<b>5</b>	<b>Discussion</b>	<b>41</b>

# 1 Introduction

## 1.1 A glimpse into the first moments after the Big Bang

How did the universe develop from the Big Bang to its current state? Physicists have been asking themselves this question for decades. ALICE (an acronym for A Large Ion Collider Experiment) is a special particle physics experiment designed to give a better understanding of the first microseconds after the Big Bang. It is located at the European Organization for Nuclear Research (CERN) near Geneva, Switzerland, and set up at CERNs largest circular accelerator, the Large Hadron Collider or short LHC. For about ten months every year, the LHC accelerates only protons to collide them at total center-of-mass energies up to  $\sqrt{s} = 14$  TeV. But about one month every year, the LHC accelerates fully ionized lead atoms, producing so-called heavy-ion events. This is where the strength of the ALICE experiment comes into play, because it has been designed to cope with the high particle production rate of lead-lead collisions. In order to understand why the observation of heavy-ion collisions is important for physical research, one has to take a brief look into the field of particle physics called quantum chromodynamics (or QCD).

QCD is a quantum field theory that describes one of the fundamental forces, namely the *strong interaction*, which is the interaction of quarks and gluons, particles that carry color charge. A characteristic trait of the strong interaction is its functional dependence of force and distance, e. g. between a quark and an antiquark that form a bound state. The force between the two particles is often compared to the stretching of a polymer or rubber band: While for small distances well below the proton radius  $r = 0.9$  fm the force acting on the particles is vanishing (*asymptotic freedom*), for higher distances the force enlarges with distance. In this sense, the strong interaction behaves oppositely to the electromagnetic force which decreases with distance. The rubber band tears apart at a critical distance; the critical energy of the bound state, on the other hand, is so high that it is energetically favorable to spontaneously produce a quark-antiquark pair and form two new bound states. This is the reason why quarks always appear in bound states. The phenomenon is called *confinement*.

During the first moments of the existence of our universe, at timescales of about 1-10  $\mu$ s after the big bang, all matter that existed was in a state of extremely high energy density, large compared to nuclear matter energy densities  $\epsilon_0 \simeq 0.15$  GeV/fm<sup>3</sup> [1]. At these conditions, quarks and gluons are expected to be free and appear in a new, deconfined phase called the quark-gluon plasma or QGP. The actual energy density for the transition from the hadronic to the plasma phase is subject of current research; recent QGP lattice calculations indicate a critical energy density of about 1 GeV/fm<sup>3</sup> [1]. At vanishing baryon chemical potential<sup>1</sup>, the (pseudo-)critical temperature is estimated to be in the range of 155-160 MeV<sup>2</sup> [1].

---

<sup>1</sup>a measure of the energy change by the addition of another baryon to the system

<sup>2</sup>A particle physics convention is to express temperatures in terms of energies by multiplying Boltzmann's constant,  $k_B = 8.617 \cdot 10^{-5}$  eV K<sup>-1</sup>. The aforementioned temperature is thus equivalent to  $2 \cdot 10^{12}$  Kelvin.

But statistical physical quantities such as energy density or temperature can only be defined for a system that consists of a large number of particles (order of magnitude  $10^4$ ) that reaches a local equilibrium at least approximately and temporarily. This means the system's lifetime has to be significantly larger than the inverse rate of interactions, so that statistically a minimum interaction rate of approximately 5 interactions per particle occur [2]. This is relevant when physicists aim at reproducing the QGP experimentally in particle accelerators: Particle collisions are well suited to achieve high energy densities and temperatures, still proton-proton collisions produce too few particles to fulfill the requirement of an equilibrium state. On the other hand, lead-lead collisions produce an abundance of particles, for instance the ALICE experiment is able to record around 3000 particles per collision at current center-of-mass energies per colliding nucleon pair  $\sqrt{s_{NN}} = 5.5$  TeV, enough to temporarily produce the QGP [6].

## 1.2 The ALICE experiment

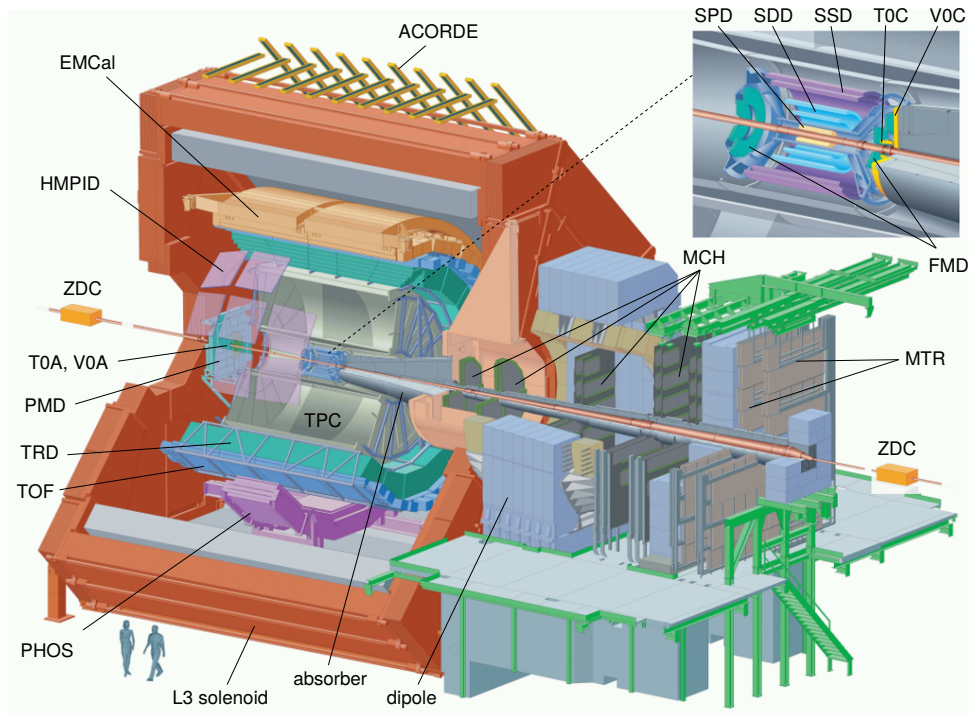


*Figure 1:* Schematic view on the ALICE experiment. Taken from [4].

As motivated in the last section, physicists want to produce the quark-gluon plasma in order to measure its properties and signatures. These measurements are the main purpose of the ALICE experiment. Thus, it has been designed to cope well with the special requirements (in particular, high particle production rate) of heavy-ion collisions. A schematic view on the experiment setup is shown in Figure 1. The detector parts are organized in the shape of a barrel with total dimensions 26 m x 16 m x 16 m and an overall

weight of 10.000 T [7]. The individual detectors are now described in ascending order of their distance to the interaction point.

The *Inner Tracking System* (ITS) is a silicon detector composed of six layers that surround the beam pipe. Its main purpose is the high precision determination of the primary and secondary decay vertices. The ITS is enclosed in the *Time Projection Chamber* (TPC), a drift chamber that is used for reconstruction and particle identification. The TPC is the most relevant detector for this thesis; it is described in detail in Section 1.3. The following detector is the *Transition Radiation Detector* (TRD). It gives additional track information and supports electron identification. On the next layer is the *Time-Of-Flight* detector (TOF) which mainly serves for particle identification. It is enclosed by two electromagnetic calorimeters, *EMCal* and the *Photon Spectrometer* (PHOS), a Cherenkov detector called *Ring Imaging Cherenkov* detector (RICH), and the *High-Momentum Particle Identification Detector* (HMPID). All detectors named so far are so-called *central barrel detectors*. They are contained in a solenoidal magnet that provides a magnetic field of approximately 0.5 Tesla [7].

In axial direction of the detector there are additional, smaller detectors, used for triggering and further event characterization; they are the *Zero Degree Calorimeter* (ZDC) and the *Photon Multiplier Detector* (PMD) as well as the three detectors that form up the *Forward Detector* (FWD), V0, T0 and the *Forward Multiplicity Detector* (FMD). Finally, the *muon spectrometer* aims on detecting muons with low transversal momentum. In the ALICE coordinate system, the z-axis is aligned with the beam pipe pointing opposite to the muon spectrometer, the x-axis is aligned to the local horizontal and the y-axis to the local vertical. For the purpose of this thesis, only the Time Projection Chamber is explained in more detail. For a comprehensive explanation of the other detectors, consult [7].

### 1.3 The Time Projection Chamber

The Time Projection Chamber is ALICE's has two important tasks: First, the reconstruction of the three-dimensional particle track that is bent due to the magnetic field inside the TPC. Secondly, the particle identification by the determination of the particle's energy loss per length  $\frac{dE}{dx}$  which can then be used to identify the particle with help of the *Bethe-Bloch formula*. The strength of the TPC lies in the capability of coping with up to 20.000 primary and secondary<sup>3</sup> particles per event [6].

The basic shape of the TPC is a sealed cylindrical container filled with working gas. It measures 5 m in length and 5 m in diameter, resulting in a gas volume of about 90 m<sup>3</sup>. Figure 2 (left) shows the components of the TPC: In its middle and azimuthally surrounding the interaction point is the *central high voltage cathode*. It is approximately 30  $\mu$ m thick and divides the gas volume equally. Next to it on both sides are the *drift volumes*. They are enclosed in the *outer field cage* which together with the cathode generates a highly

---

<sup>3</sup>Primary particles are produced as direct consequence of the collision, while secondary particles are decay products of the primary particles.

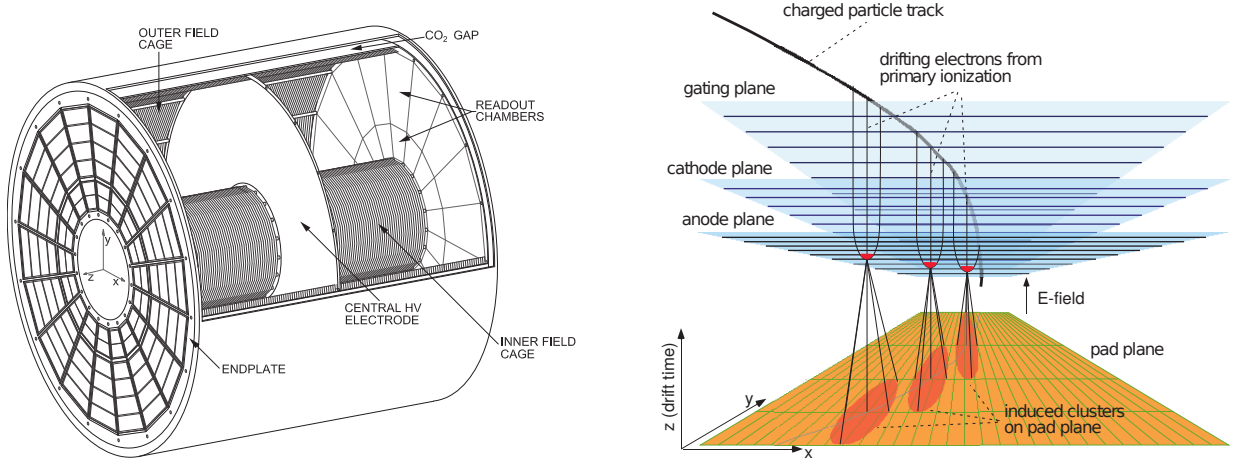


**Figure 2:** Left: A sketch of the ALICE Time Projection Chamber [3]. Right: Schematics of a multi-wire proportional chamber [12].

homogeneous electric field of the size  $E = 400 \text{ V/cm}$ .<sup>4</sup> The TPC is closed off on each side by the readout end plates. They are (as typical for ALICE) segmented in 18 trapezoidal elements. Each one of them is again subdivided in Outer Read-Out Chamber (OROC) and Inner Read-Out Chamber (IROC).

The setup of the readout chamber, operated by a Multi-Wire Proportional Chambers (MWPC), is sketched in Figure 2 (right). It consists in planes of parallel wires: A gating plane (*gating grid*) which can open or close the readout area, the anode and cathode planes which generate an amplification field and the segmented cathode plane (*pad plane*) which can be read out by electronics. In the following, the physical process and the meaning of the components are described in more detail.

After the collision of particles in the interaction area, generated particles (around 3000 for Pb-Pb collisions) cross the TPC area. Focusing on only one produced particle that crosses the TPC, the following processes can be divided into four general steps:

1) **Electron-ion-pair generation:** Due to the interaction of the high-energetic particle with the working gas, it ionizes gas molecules. As only a small fraction of the particle's energy is needed for that, the particle continues on its track, leaving ions and electrons along his way. Because of the magnetic field  $B \simeq 0.5 \text{ T}$  in the central barrel area, the particle track is bent, allowing to measure its momentum later on. The detection of the produced electrons will enable the reconstruction of the particle track.

2) **Electron drift:** The electrons now drift towards the anode; *drift* describes the process of traveling through a medium under the influence of an electric field. The homogeneity of the field ensures that the lateral ( $xy$ -)movement of the electrons are minimal. The drift velocity is mostly dependent on the mean time between collisions with gas molecules  $\tau$  and can be approximated with Townsend's formula  $w = \frac{e}{2m} E \tau$  [9]. Here,  $m$  denotes electron mass,  $e$  electron charge and  $E$  electric field size.  $\tau$  is dependent on the collision

<sup>4</sup>The ITS is shielded from the field by the *inner field cage*.

cross-section and thus on the gas type, pressure and temperature as well as on the electric field  $E$  itself. As a consequence, the macroscopic velocity of the electrons can be described as constant for fixed gas mixture and electric field. In the TPC, an electron needs about 92  $\mu\text{s}$  to travel the full distance in  $z$ -direction in a gas composition of 90 % Neon and 10 % carbon dioxide.

3) **Electron amplification:** The readout chambers are composed as sketched in Figure 2 (right). The amplification area is defined by the cathode, the anode and the pad planes. The particles in this area are accelerated and gain in energy. For energies above 100 eV [9], They are able to ionize gas molecules, creating more free electrons that can in consequence ionize further molecules (*avalanche effect*). For a high enough voltage difference between cathode and anode<sup>5</sup> the produced charge is proportional to the original charge; in the TPC there is a factor of about  $2 \cdot 10^3$  [12].

4) **Signal generation:** The ions created in the avalanche process drift back towards the cathode wires and meanwhile induce a mirror charge on the pad planes high enough to create an electronic signal. The geometry of the wires is chosen in such a way that a signal in average spreads over three pads. This makes it possible to determine the  $xy$ -position of the primary electron with a higher resolution than the actual pad size. The electrons generated during that process have a drift velocity approximately three orders of magnitude higher than the ions; thus they are fast absorbed by the anode and their contribution to the signal is negligible [12]. By combining timing information of the generated signal and drift velocity in the gas, it is possible to determine the  $z$ -coordinate of the particle track where the primary electron was produced.

The large production of ions is a negative consequence of the above mentioned avalanche effect. If not stopped, the ions travel back towards the drift volume and can accumulate there. This might lead to distortions of the electric field. The aftereffect would be a severe loss of reconstruction ability, which is why the *gating grid* was introduced, another wire plane that can separate the drift volume from the amplification area. The separation is achieved by applying positive and negative potential on the wires in an alternating manner. Both incoming electrons and back-flowing ions are then drawn to the gating grid wires and neutralized there.

Following particle collision, the gating grid opens for the time duration that drift electrons need to cross the full TPC length (about 92  $\mu\text{s}$ ). The gate is then closed to block ions flowing back to the drift volume; this also leaves the detector blind to any further particles crossing the drift area, meaning another collision during this interval could not be recorded. This forced rhythm dictates the rate in which particle collisions can happen, 8 KHz for lead-lead collisions in Run II. However, in Run III, the collision rate of the LHC is increased to 50 kHz [3]. To ensure the accustomed high performance of the detector at this interaction rate, an upgrade is needed for the TPC.

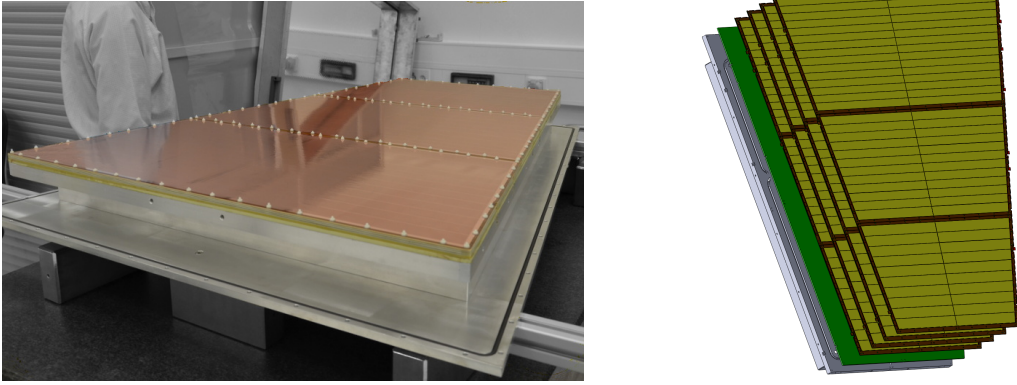


**Figure 3:** Left: Pre-assembled outer readout chamber prototype (OROC). Most prominent in the photo is the tripartite coppery GEM and the aluminium frame (*alubody*). Right: Exploded schematic view of one of the 18 trapezoidal OROCs. From rear to front it is shown: The alubody, the fiberglass support plate, the pad plane and a stack of four gas electron multipliers (GEMs). The GEMs are vertically divided into three parts called OROC 1, 2 and 3 (from bottom to top), which are in turn subdivided into segments [3].

## 1.4 The Time Projection Chamber Upgrade

The increase of interaction rate in Run III motivates a change in technology concerning the electron amplification domain. The ALICE collaboration decided to replace the multi-wire proportional chambers by chambers with Gas Electron Multipliers (GEMs). GEMs feature intrinsic ion backflow blocking properties which provide the means of electron amplification by a factor of around 2000 at now *continuous* readout of events, a major improvement to the current setup based on the gating grid. This technological upgrade implies other improvements and adjustments: The readout electronics need not only to accommodate a change of polarity in the signal, but also to an expected average data rate of 1 TByte per second. This leads to high requirements in data compression to match the anticipated data bandwidth for permanent storage. A comprehensive review of the new requirements and the upgraded parts of the Time Projection Chamber Upgrade (TPCU) can be found in [3].

Most parts of the current TPC are reused in the upgrade, including the field cages, the gas system and the service components. The 18 trapezoidal readout chambers, however, will be completely produced again. Figure 3 (left) shows an outer readout chamber (OROC); the prototype on the photo has been pre-assembled at the *GSI Helmholtz Center for Heavy Ion Research* (GSI) in Darmstadt, Germany. Figure 3 (right) shows the main components of the chambers: The aluminium frame (*alubody*), which provides gas tightness and physical stability to the chambers and accommodates the readout electronics, the support plate and the pad planes that detect electronic signals and four layers of GEM foils that serve for electron amplification. The production includes the following important steps: the production of the alubody, the pad planes, GEM foils and their quality assurance (QA),

---

<sup>5</sup>The line charge density has to be too large compared to the charge density of generated electrons.

the assembly of the readout chambers and finally the integration into the TPC.

This thesis is focused on the GSI's involvement in the quality assurance of the GEM foils, which is in particular one of the two main quality tests, the leakage current measurement. A theoretical introduction on the electron amplification with GEMs, on the TPCU GEM design and the production processes are given in Chapter 2. A detailed description of two essential processes of foil handling done at GSI, namely the GEM frame gluing and the leakage current test, are given in Chapter 3. The analysis of a number of measurement sets conducted with the leakage current measurement in Chapter 4 is the main part of the thesis; more precisely, the impact of a number of variables on a foil's leakage current is examined. A discussion of the analysis results and the leakage current test as well as some suggestions for future research and improvements conclude this thesis in Chapter 5.

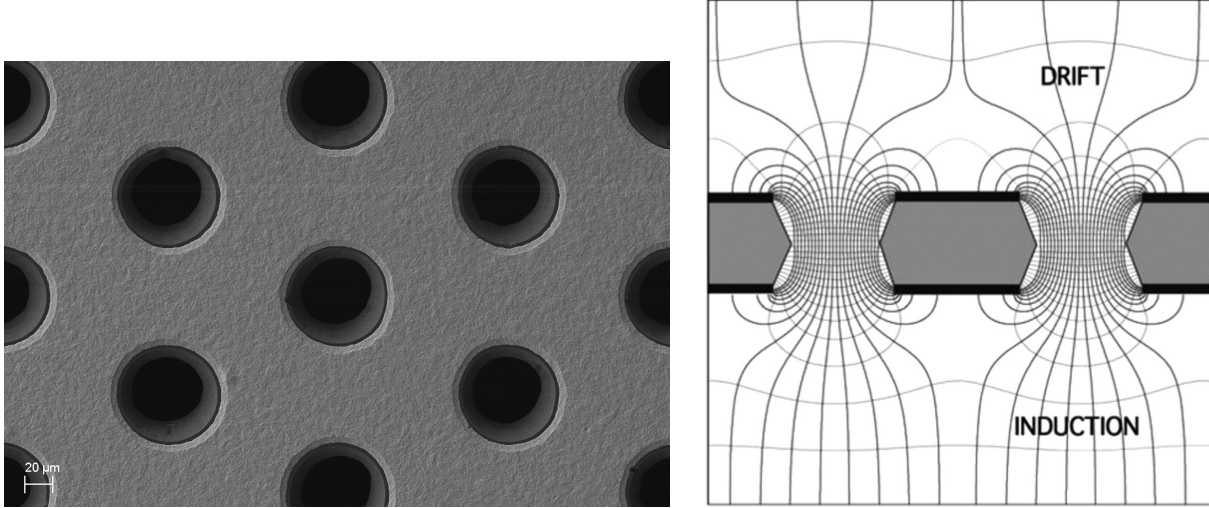


**Figure 4:** Left: Microscopic view on a GEM foil. The holes are arranged in a hexagonal manner. Also visible is that the hole diameter varies with depths [3]. Right: A sketch of the electric field produced by the GEM foil. It is noticeable that the field lines direct the electrons into the holes, where there is a high line density and a strong electron acceleration. The electric field is higher below the GEM because there is an element with higher positive voltage below [11].

## 2 Introduction to Gas Electron Multipliers

### 2.1 General approach to Gas Electron Multipliers

The beforehand chapters have been focusing on the processes in the Time Projection Chamber that can be divided into the four general steps of electron generation, electron drift, electron multiplication and signal detection. In the current TPC setup, a multi-wire proportional chamber provides the means for electron multiplication and signal generation. GEM technology replaces the MWPC in the TPC upgrade: GEMs perform the task of multiplying the ionization electrons; in comparison to the MWPC, where mirror charges of ions induce currents in the pad planes, with GEMs the produced electrons drift directly towards the pad plane, where they are absorbed and produce currents high enough to be measured.

A GEM foil, as shown in Figure 4 (left), is an approximately  $50\ \mu\text{m}$  thin, metal-clad polymer foil. The GEMs examined in this thesis consist of a Kapton core clad by copper on both sides. Kapton is a strong insulator which can withstand even strong electric fields. This foil is processed by lithography to chemically perforate it. A typical foil, the so-called ‘standard’ GEM, has around 100 holes per square millimeter with a diameter of  $70\ \mu\text{m}$  and a pitch size (distance between centers of adjacent holes) of  $140\ \mu\text{m}$ . The so-called ‘large’ GEM has the same hole diameter but an increased pitch size of  $280\ \mu\text{m}$  [10]. As a result, the GEM foils appear slightly transparent when held against a light source. The GEM production process resembles the etching of double-sided printed-circuits. Due to the way the etching process works, the holes’ sides are not perfectly flat but rather

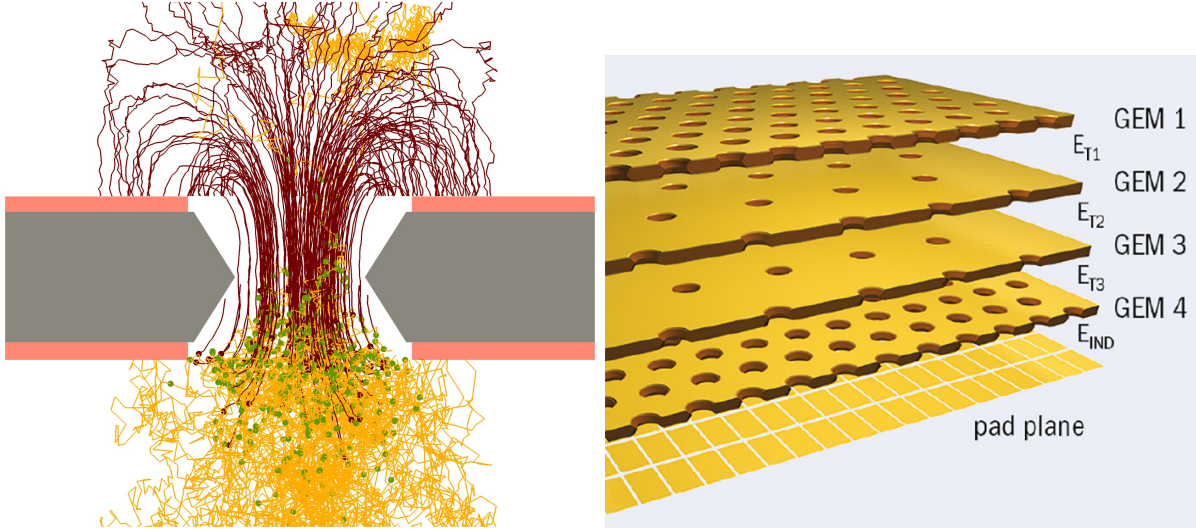


**Figure 5:** Left: A simulation of electron multiplication and ion production in the holes of a GEM foil. Electron paths are drawn in yellow, ion paths in orange and the production spots with green dots. A certain ion backflow reduction is visible [5]. Right: A visualization of the GEM foil stack. Top and lower foil have ‘standard’ hole size and pitch, while the second and third GEM have ‘large’ pitch size. The distance between adjacent GEMs is 2 mm [3].

double-conical as can be seen in Figure 4 (right). Their diameter varies between 70  $\mu\text{m}$  at top and bottom of the foil and about 50  $\mu\text{m}$  in between.

GEM foils are typically installed in the gas-filled drift areas between drift and collection electrode. When a voltage difference between the two copper layers is applied, it results in a strong electric field in the holes (due to the voltage difference over the small distance). To understand which effect this is imposing on drift electrons, it is best to look at the field lines shown in Figure 4 (right). Electrons that arrive in front of the foil (upper part) are drawn into the GEM holes, an appropriate choice of voltages assumed. The dense field lines show the expected high electric field, causing a rapid acceleration of the electrons. The gain in kinetic energy and the interaction with the gas causes electron multiplication and avalanches: the drift electrons ionize gas molecules when they hit them with energies above 100 eV. The result is a gain of electrons of the order of magnitude of  $10^2 - 10^3$ . What is even more, in their amplification GEMs preserve the original electron xy position. Each hole serves as an independent amplifier, screened from the other holes and only lightly affected by external fields [10]. As a result, the GEMs work as electron multipliers and signal amplifiers.

## 2.2 The TPCU GEM design

In experimental implementations of GEMs, one has to bear in mind that each produced electron leaves behind a positively charged ion that drifts towards the cathode. This effect (called *ion backflow*) has no severe impact when there are only few ions created, like for the crossing particle and the primary generation of charges. But in the holes

of the GEMs there is such an abundance of ions produced that they form space charge which can significantly distort the electric field. Though, the drift chamber relies on a homogeneous electric field; agglomerations of ions will draw drift electrons towards them and disturb their xy-localization. Therefore, special attention was payed to the reduction of ion backflow was in the design of the TPC upgrade GEMs. Simulation studies found that the detector performance would see tolerable losses if the ion backflow could be kept as below 1 %, meaning of one hundred produced ions only one ion flows back to the drift region [3].

It is a unique feature of GEMs that several of them can be cascaded in the same detector, thereby reaching an *effective gain* that is the product of the individual gains. With clever alignment, the stacking can also reduce ion backflow drastically by exploiting the huge mass difference between electrons and gas ions: If holes of subsequent GEMs do not overlay in their xy-position, only lightweight particles can change their momentum fast enough to pass through the GEM holes. So, while most electrons flow further downstream and are collected by the pad plane, the ions move towards the negatively charged foils and absorb electrons from the surface, thereby being neutralized.

In a major research and development operation, it was found that a stack of four GEMs is necessary to meet the specifications. Their parameters have been varied to minimize ion backflow and to optimize energy resolution and uniformity of gain over the whole GEM area. Adjustable parameters are voltages on both sides of the four foils, hole diameters, pitch sizes (distance between two adjacent holes), hole alignment and hole orientation. In the end, it was decided on an array that can be seen in Figure 5 (right): It uses a mixture of ‘standard pitch’ GEMs (pitch size 140  $\mu\text{m}$ ) for the top and bottom GEM and ‘large pitch’ GEMs (pitch size 280  $\mu\text{m}$ ) for the middle foils in the stack. Also, the hole alignment of the first and third layer (GEM 1 and GEM 3) is rotated by  $90^\circ$  to minimize the hole overlay of adjacent GEMs [3].

The production of a GEM foil large enough to cover the whole readout chamber is not possible yet. Thus, multiple GEMs are used to span the area, one for the IROC and three for the OROC. The GEMs themselves are further segmented on their front side (between 18 and 24 segments). They are connected to a high voltage distribution trace via decoupling resistors that ease the effects of potential discharges. Each segment is supposed to have an area of approximately  $100\text{ cm}^2$ .<sup>6</sup> The GEM bottom is not segmented and can thus directly be connected to high voltage. The GEMs that will be referred to in this thesis can be distinguished by their OROC number from 1 to 3 (the vertical division in Figure 3) and their GEM number from 1 to 4 (the position on the stack in Figure 5).

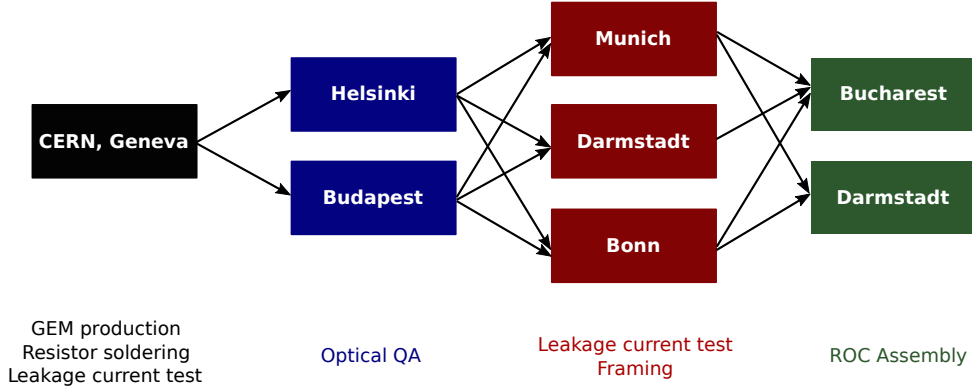


**Figure 6:** Material and work flow for OROC GEMs.

### 2.3 Main steps for quality assurance and the GEM production chain

The largest time projection chamber of the world is upgraded to deliver a continuous signal; the enormous effort carried out by the ALICE collaboration is evident. Several physics institutes all over the world are involved in the production of the new readout chambers. A few key points of the work flow shall be explained in the following: There is a general division in the production of IROCs in the United States and OROCs in Europe; for this thesis it is sufficient to look at the OROC GEM production in Europe which is illustrated in Figure 6. The GEM foils are produced at CERNs PCB (Printed Circuit Board) workshop and then split and shipped to the *Helsinki Institute of Physics* and the *Wigner Research Center for Physics* in Budapest, where their quality is assured by an automated optical examination. Subsequently, they are shipped to the *Technical University of Munich*, the *University of Bonn* and the *GSI Helmholtz Center for Heavy Ion Research* in Darmstadt. There the foils undergo a quality assurance in form of a leakage current measurement and they are glued to their frame after which follows another leakage current measurement. The readout chamber assembly (body and GEMs) is done at the *National Institute for Physics and Nuclear Engineering* in Bucharest and at the *GSI* in Darmstadt. The final mounting onto the TPC takes place at CERN.

---

<sup>6</sup>This limits the capacity of the segment; empirical findings indicate that this eases the effects of possible discharges.

## 3 GEM handling processes at GSI

### 3.1 General GEM safety tips

GEMs are highly sensitive and susceptible objects since they have to withstand high voltage differences over only a few micrometers. Even a contamination with tiny dust particles can result in discharges and short circuits between the two foil sides; thus GEMs can only be handled in clean room conditions. The obligatory protective clothing for all clean room workers includes a clean room overall, clean room shoes, a protective hood and, if applicable, beard protection. When in direct contact with GEMs, a mask covering mouth and nose and gloves are also mandatory.

GEMs must always be treated with highest attention and care. In general, two persons handling the GEMs increase the safety and reduce mistakes. Tools should never be passed and persons should never lean over the foils. Further, it is important to clean all equipment and worktops that come near the GEM. For that purpose, isopropanol or ethanol together with lint-free cloths are eligible, acetone must not be used. Compressed air can supplement the cleaning of equipment and foils in form of blowing clear from dust. In case of an incident with a GEM, a thorough documentation in the database is important.

### 3.2 The leakage current measurement

The leakage current measurement is a electrical characterization of the GEM foils. Its basic idea is the following: The bottom side of the GEM is connected to a ground potential while the top side is put on a high negative voltage; an ampere meter measures the current flowing from the bottom to the top side for each segment. In practical application, the measurement is more complicated, for instance due to high requirements on the GEM quality. The reason for these requirements is that the foils operate in an area where there is a high rate of high-ionizing particles. This causes an increased likelihood of gas discharges which can in turn cause short circuits between the foil sides. It has been found that the risk of a GEM damage during operation is satisfactorily low when the leakage current per segment without radiation but under a voltage difference of 500 V is below  $I_{\text{limit}} = 0.5 \text{ nA}$  [8]. The leakage current changes with gas composition and humidity, thus the test is conducted in nitrogen for which above value of  $I_{\text{limit}}$  was determined. The following chapters give more details on the used test equipment, the test setup and the testing procedure. They are supplemented with the images (a)–(l) found in Figures 7–11.

#### 3.2.1 Testing equipment

1) **The test drawers.** The main purpose of the drawers is to deliver an easy, fast and safe way to connect the measurement equipment with the GEM foil. There are three different testing drawers that correspond to the three OROC types. Each drawer consists of two acrylic glass plates of the size of approximately 120 cm x 80 cm. The bottom plate

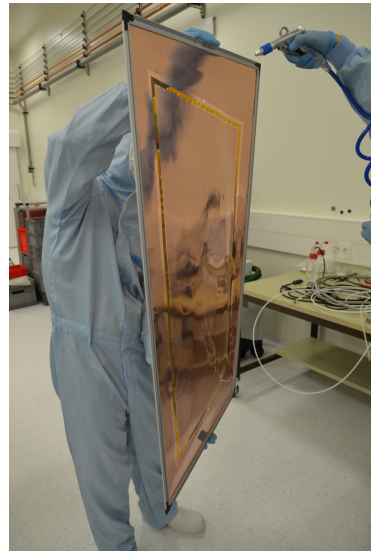


**Figure 7:** (a) foil storage dry cabinet, (b) taking foil out of paper bag, (c) cleaning foil with compressed air

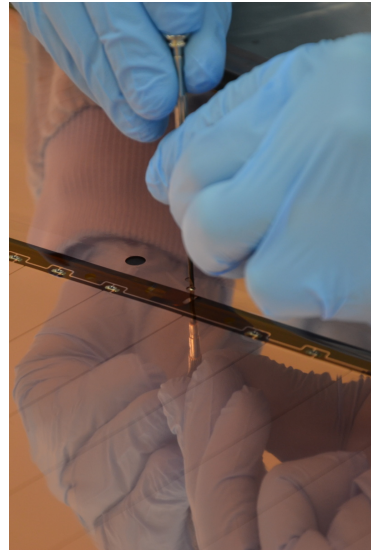
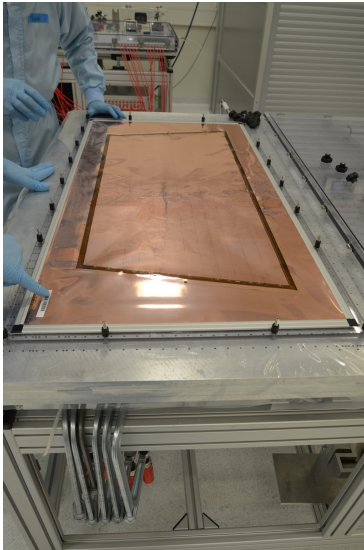
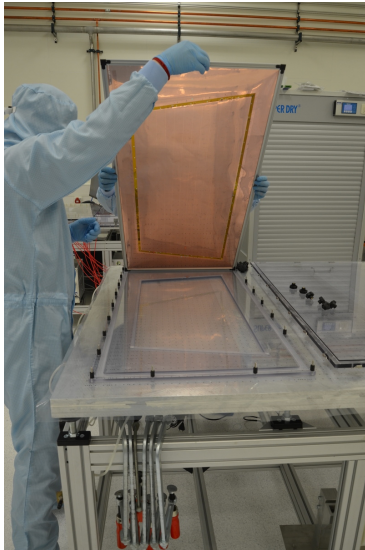


**Figure 8:** (d) placing foil in drawer bottom plate, (e) foil placed in bottom plate, (f) turning ground connection plate

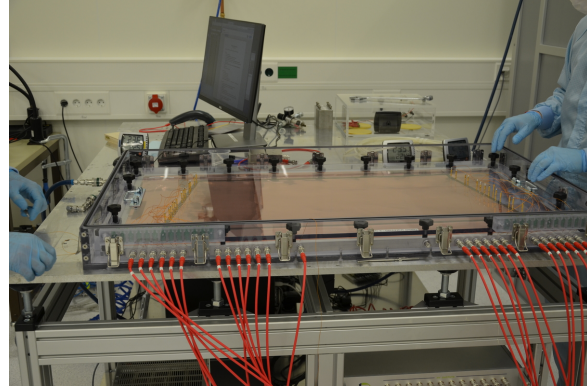
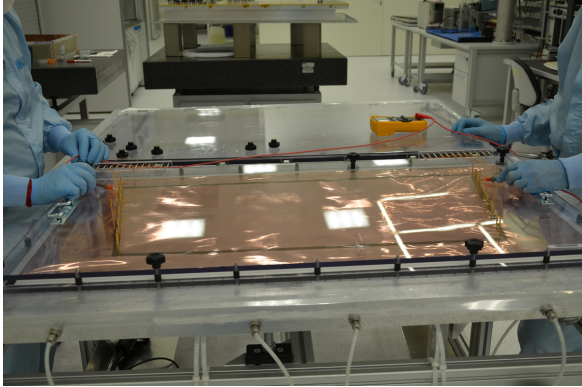


**Figure 9:** (g) connectivity check, (h) drawer inserted in test box

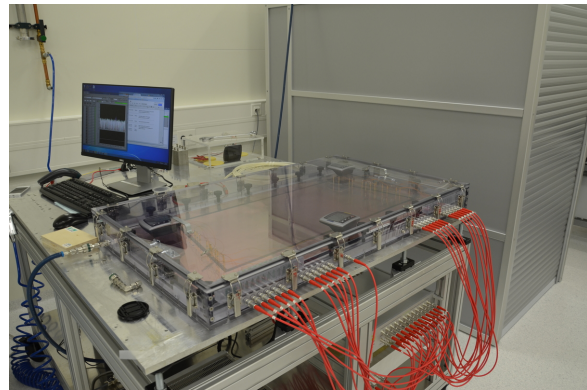


**Figure 10:** (i) ground connection, (j) closed test box

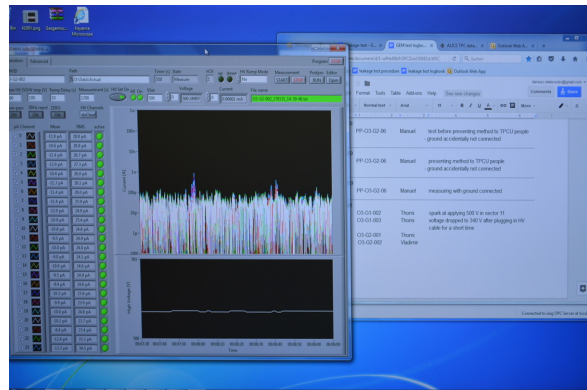


**Figure 11:** (k) hygrometer in the test box, (l) LabView measuring program and logbook

has a cut-out in the shape and size of the active GEM area. The foil can be placed on the bottom plate with its ‘optiguard’<sup>7</sup> frame placed on the corresponding notches on the plate. The top plate is mounted on top of the bottom plate and foil; spacers of about 2 cm prevent the top plate from touching the foil. Top and bottom plate can be combined with black screws (see Figure (g)). On the bottom side of the top plate there are pins that establish the electrical connection to the segments of the foil, the HV path and the ground connection. The pins can change in height due to spring suspensions. On the top side, each pin is connected by a wire to a corresponding spring pin on the side of the drawer which in turn connects the drawer to the test box. Two more details shall be explained: The drawer can be used for both framed and unframed GEM foils. In order to compensate for the height difference of the frame, there is another notch in the bottom plate that can either accommodate the foil frame or can be padded up with a dedicated plastic frame when the foil is not yet framed. Furthermore, there is a small copper plate on the bottom plate that can be used to establish the connection to the foil bottom with a pin from the top plate.

**2) The test box.** The test box provides the means to test the foil in a controlled environment. It is a gas-tight acrylic glass box equipped with a gas inflow and a gas outflow connection and 26 coaxial cable plug sockets (for 24 segments, the HV connection and one spare). Each coaxial plug socket is connected to a contact face on the inside of the box which can connect to the pins on the side of the test drawers. The top plate of the test box can be removed in order to place or remove the test drawer.

**3) The HV source.** In the current test setup, one HV source is sufficient to deliver the negative voltage of  $U_{\text{HV}} = 500 \text{ V}$ .

**4) The ampere meter.** The 24-channel ampere meter with a resolution of 0.1 pA serves in measuring the leakage current. It is also called picoammeter.

### 3.2.2 The test setup

A wiring diagram of the experiment setup can be seen in Figure 12. On the right-hand side, we see the ground potential that is connected to the bottom side of the GEM. In the setup, it is delivered by the HV source, connected to the inside of box via the coaxial cables and brought to the GEM by a pin that touches a copper plate underneath the foil. As visible in the diagram, the GEMs are best described by a capacitor with a capacity of about  $C_G \approx 5 \text{ nF}$  [3]. They do not act as a perfect capacitor as a small current on the scale of pico amperes travels through the holes of the GEMs, the leakage current.

In earlier stages of the GEM production process, there are no decoupling resistors present between the segment and the HV supply path on the foil. The leakage current can then be directly measured between HV source and segment. When the resistors are placed, however, the leakage current is measured in serial connection to the decoupling resistors as visible in Figure 12. The leakage current splits between the two resistors, for a derivation of the formula see Chapter 24. In the setup, the wiring is slightly different from the

---

<sup>7</sup>The outer metal frame which supports the foil.

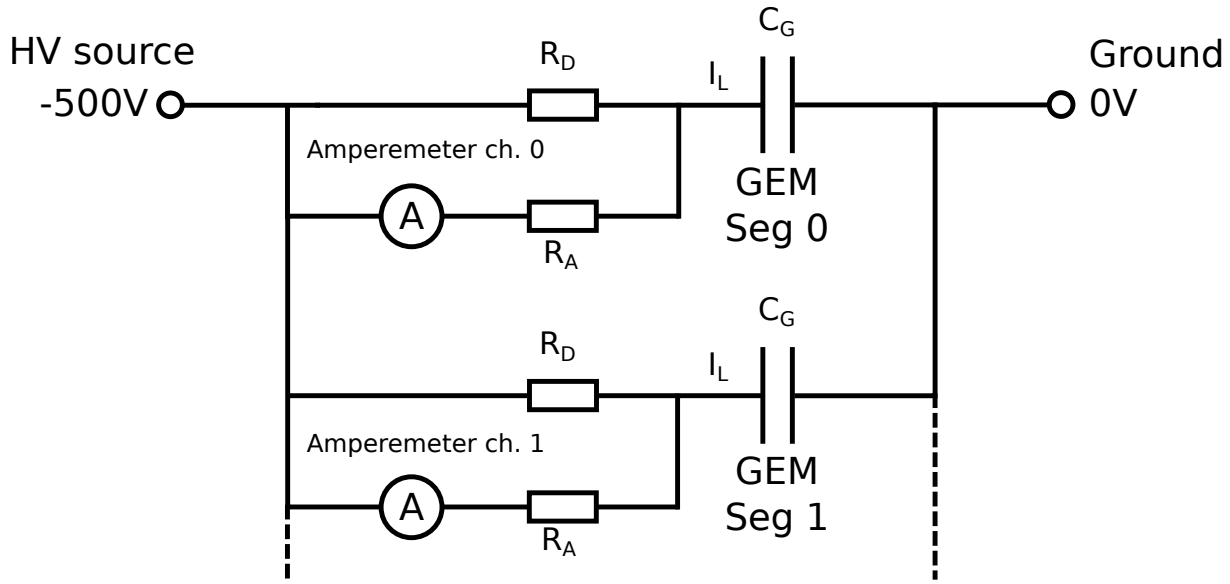


*Figure 12:* Wiring diagram of the leakage current test.

wiring diagram: The decoupling resistors are connected to the HV path which has a direct connection to the HV source. The connection to the ampere meter goes via the drawer pins that touch the segments on the solder of the resistors to the ampere meter which is located outside of the test box. The ampere meter is itself connected to the HV source.

### 3.2.3 The testing procedure manual

**Preparation.** At least one free table is necessary. It has to be cleaned adequately, optionally covered with a plastic foil. The drawer and test box need to be cleaned. Mouth and nose masks and gloves are mandatory.

**The test drawer.** The test drawer is placed on the table. The screws that connect top and bottom plate are unscrewed and the top plate is removed. Special care has to be taken in order not to damage the pins when placing the top plate at another location. If the test foil has a frame, the plastic substitute on the drawer has to be removed. If the test foil is not yet framed, the plastic substitute has to be placed in the corresponding notch. This is necessary in order to ensure that the spring-suspension pins do not bend the GEMs.

The foil is taken out of the dry cabinet (a) and retrieved from the paper bag (b). Two persons are recommended for this task to minimize any forces acting on the foil. The foil is then cleaned using compressed air (c). Any potential dust is blown away from the top to the bottom towards the floor. The GEM is placed on the bottom plate of the drawer (d). The metallic ‘optiguard’ frame is placed in the corresponding notch on the bottom plate (e). The paper bag is stored in a clean location. On one side, a few millimeters next to the dark brown Kapton area, there is a small hole in the foil through which the

copper plate can be seen. With the help of a small slot screwdriver, the copper plate is turned and inserted in the small gap between foil and frame (f). When removing the foil after the test, it is important to remember to undo this operation before lifting the foils. Otherwise, undesirable forces act on foil, frame and glue.

The top plate of the acrylic glass is put back; even though the risk of puncturing the foil has been reduced due to the usage of flat-head pins, it is still important to lower the top plate as gently as possible. It is recommended praxis to attach a few screws only and check with a multimeter whether all pins are connected correctly (g). The resistance between HV path and the segment connection is  $R = 5 \text{ M}\Omega$  for GEM 1-3 and  $R = 1 \text{ M}\Omega$  for GEM 4. Additionally, an infinite resistance between HV path and ground is expected. After attaching the remaining screws (applying only little force<sup>8</sup>), the drawer can be inserted into the test box (two persons recommended). The best way to insert the drawer is to first lower the pin side of the drawer onto the floor of the test box and then shove it towards the contact faces. From there the drawer can be lowered entirely (h).

**The test box.** Once inserted, two more connections have to be set up: The pin touching the copper plate has to be connected to the test box ground using crocodile clips (i) and the test box HV clip has to be connected to the HV path pin. The test box is then further equipped with three digital hygrometers (not to be placed above the foil bar code). The test box can be closed (j) and flushed with nitrogen until the absolute humidity in the test box is below 3000 ppm. For the stable clean room conditions, this corresponds to a relative humidity of about 10%. The humidity conditions can fluctuate inside the test box, so a value below 10% has to be reached on all hygrometers. With steady gas flow, the test can be started (k).

**The leakage current test.** The voltage is set to  $U_{\text{HV}} = 0 \text{ V}$ . It has to be checked that there are no unusual currents flowing, for example from a former charging of the foils. The recording of measurement values is started. The computer stores one current value per segment per second and additionally, the voltage and current output of the HV source. After a few seconds of plain and uncorrected measurement, the current offset of each channel is determined by averaging over 2s of leakage current measurement. This is a crucial moment for the measurement and the quality of the results obtained later on. It has to be checked that the offset has been determined correctly and with a connection to the HV source. Best praxis is to wait for about 10s and check that the currents do not fluctuate more than about 1 pA around  $I_{\text{L}} = 0 \text{ pA}$ . Another advantage of waiting is the traceability of the correct offset taking, as it is stored in the measurement file.

The connection to the HV source is then interrupted by unplugging the corresponding cable and the voltage is ramped to  $U_{\text{HV}} = 500 \text{ V}$ . By simple reconnecting the cable, the GEM reaches the high voltage in the fastest possible way (the voltage ramping of the HV source takes about 2s). The general idea behind fast ramping is that it is thought to burn away any dust that might be on the GEM, while slow ramping might cause melting and a contamination of the foil. The measurement has to be stopped and the set back to

---

<sup>8</sup>When applying force on the metal screws, they are subject to abrasion. This potentially creates metal dust which can spread and, in the worst case, create short circuits in the GEM.

$U_{HV} = 0\text{ V}$  if there are a number of visible discharges or if a segment has a short circuit. In any other case, the measurement can be proceeded. Typically, a total time of 1200 s is enough to get a reliable value for the leakage current. An example of a result for a measurement is shown in Chapter 4.1.

**Dismounting.** After the measurement, the voltage is lowered to  $U_{HV} = 0\text{ V}$ . The foil's discharge can take about five minutes and the test box should not be opened before the measured voltage has decreased entirely.<sup>9</sup> The gas flow is reduced and the box opened. The hygrometers and the crocodile clips are removed. The drawer is moved to the cleaned table and the black screws are unscrewed. The top plate of the drawer is removed carefully, the copper plate is rotated back and the foil can be lifted. It is then put back in the paper bag and stored in the dry cabinet. If not continuing with another test, the drawer is reassembled and best stored in the closed test box.

### 3.3 The framing procedure

The *framing procedure* refers to the process of gluing the polymer frame (GEM frame) to the GEM foil. The polymer frame is important in the assembly of the readout chambers; it is used to mount the GEMs on the stack above the pad planes. In the following, the relevant equipment for framing and the procedure is explained. It is supplemented with photos in the Figures 13-18.

#### 3.3.1 Framing equipment

**The gluing jig and the ‘VectorGuard’ frame (a).** These are the essential devices for gluing. The gluing jig (silver) has a notch that accommodates the polymer frame with its cross. The ‘VectorGuard’ frame (blue) is mounted on top of it; it has notches to accommodate the ‘OptiGuard’ aluminium frame that surrounds the GEM foil. When the ‘VectorGuard’ frame is supplied with compressed gas of approximately 5 bar, it releases its stretching mechanism and the foil can be inserted. Without pressure, the foil is stretched with a tension of 10 N/cm due to a spring-suspension mechanism. The relative alignment of gluing jig and ‘VectorGuard’ can be changed with the fine-adjustment turning knobs. This is used to align GEM foil and polymer frame. A special aluminium cover plate (milled such that it does not touch the active area) is used to press the foil on the frame.

**Microscope (d).** A microscope (magnification circa x100) mounted on the worktop supports the alignment of polymer frame and GEM.

**Corner pins (i).** The four metal corner pins can be inserted into the GEM foil, the polymer frame and the gluing jig. They maintain the alignment of foil and frame.

**Glue roller (f).** The glue roller supports the uniform and smooth glue spread on the frame.

**Transparent hood (l).** The transparent hood is a gas-tight cover that is placed on

---

<sup>9</sup>A charged GEM foil attracts more dust particles.

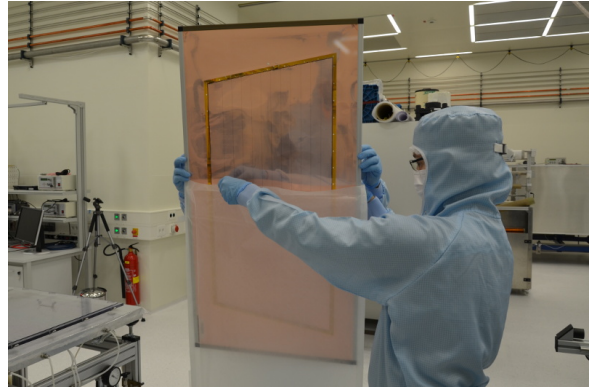
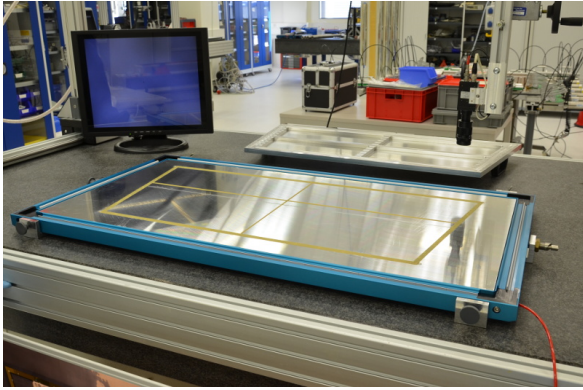


**Figure 13:** (a) gluing jig (silver) and ‘VectorGuard’ frame (blue), (b) retrieving GEM from paper bag

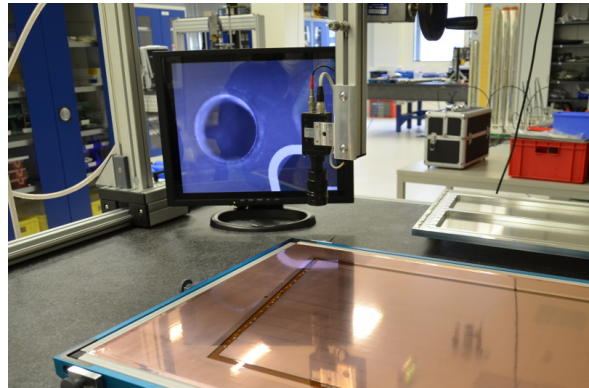
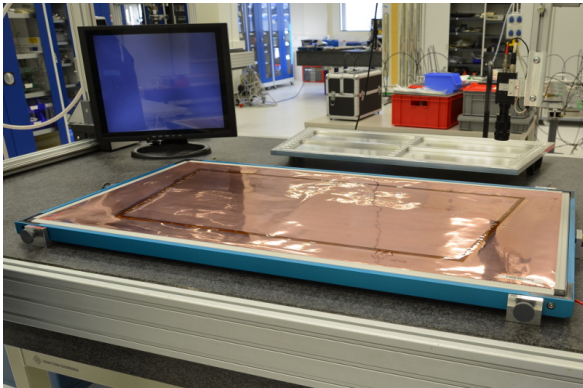


**Figure 14:** (c) the foil is placed in the ‘VectorGuard’ frame, (d) the stretched foil; the corner holes in GEM and frame are aligned with the microscope

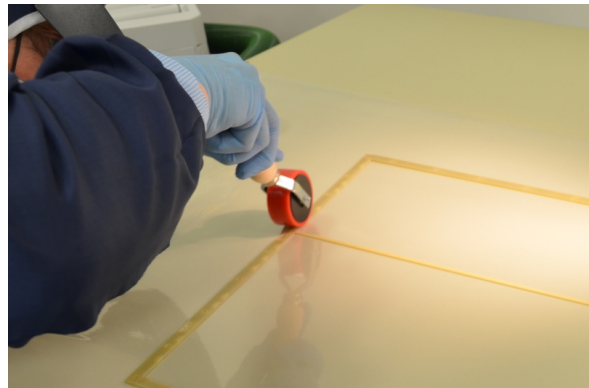
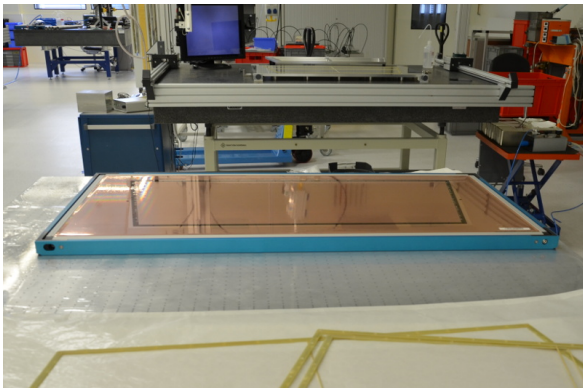


**Figure 15:** (e) the ‘VectorGuard’ frame can be moved with the stretched foil, (f) glue is applied to the frame with the glue roller

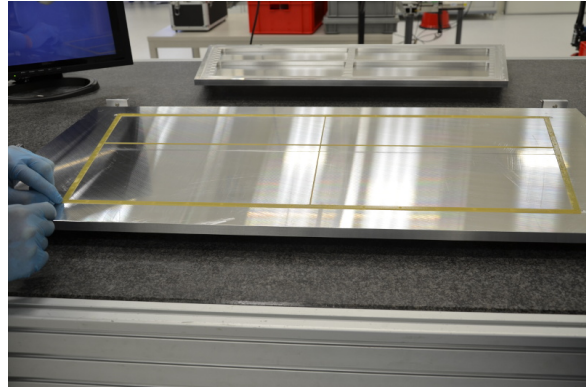
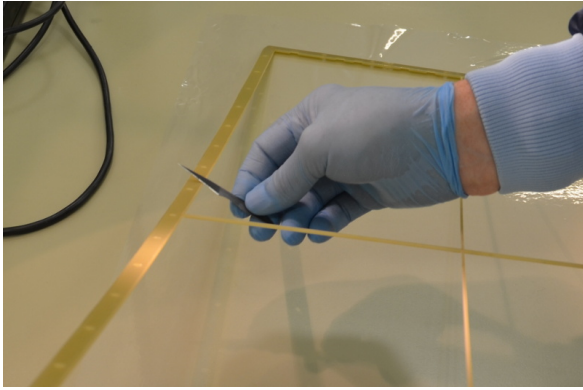


**Figure 16:** (g) the frame edges are cleaned from glue with a scalpel, (h) the frame with glue on its faces in the gluing jig

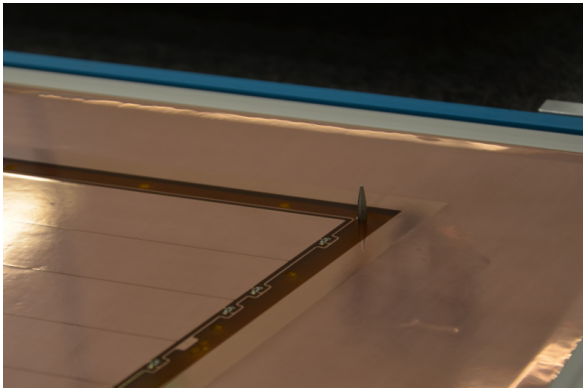


**Figure 17:** (i) the metal pins maintain the alignment of GEM and frame, (j) the gluing jig's cover plate

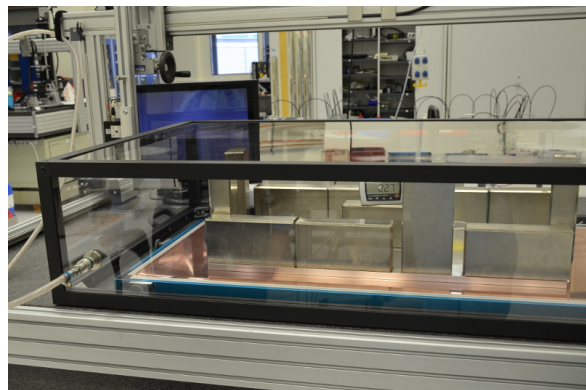


**Figure 18:** (k) the cover plate presses the GEM on the frame, (l) steel bricks apply pressure on the glued surfaces; the transparent hood covers the gluing jig and can be flushed with nitrogen

the worktop over the gluing jig. It has a gas supply and can be flushed with nitrogen to enable glue drying under optimal conditions.

### 3.3.2 The framing procedure manual

**Preparation.** The equipment is cleaned using a lint-free cloth and isopropanol. The gluing jig is placed on the table with the mounted microscope. The ‘VectorGuard’ frame is placed surrounding the gluing jig by opening the spring fastener leverages beforehand and closing them when the frame is in place. A second worktop is cleaned and covered with a plastic foil; it will be used for glue application. A third worktop is cleaned; it will be used to place the ‘VectorGuard’. The polymer frame is cleaned with an ultrasonic bath. Nose and mouth masks and gloves are mandatory.

**Alignment of GEM and frame.** The polymer frame is inserted into the notches of the inner part of the gluing jig (a). It has to be checked that the cross is well-glued to the polymer frame and that the four metal pins fit into the corner holes of polymer frame and gluing jig properly. The compressed air is connected to the ‘VectorGuard’ frame via the pressure regulator. The valve is turned to 5 bar in order to relax the stretching mechanism.

The GEM is taken out of the dry cabinet and retrieved from the paper bag (b). Compressed air is blown from top to bottom towards the floor in order to clear the foil from dust. The foil is surrounded with the aluminium ‘OptiGuard’ frame on all edges. It is placed in the notches on the ‘VectorGuard’ frame (c). The pressure regulator is turned to 0 bar in order to stretch the foil. It is disconnected afterwards; springs in the frame maintain the foil’s stretching tension.

The microscope is directed to one particular corner hole and focused on the foil (d). The frame’s hole is visible underneath as a black circle. GEM and frame are aligned by turning the adjustment screws; this in fact alters the relative position of gluing jig and ‘VectorGuard’ frame. The three adjustment screws translate their alignment in the extension of the screw axis. When one GEM hole is aligned with the frame hole, the other three have to be checked and adjusted with the microscope. From experience, it is not possible to align all corner perfectly and a trade-off has to be found. A proper alignment of a hole is characterized by the ability to easily fit in the metallic pin. When all holes are in proper alignment, the four metal pins are inserted and retrieved for a proper alignment check. It should not be leaned over the GEMS during this process.

**Glue application.** The spring fasteners of the ‘VectorGuard’ are loosened and the VectorGuard is cautiously lifted (two persons are recommended) and moved to the third worktop (e). The polymer frame is retrieved from the gluing jig and placed on the worktop prepared for gluing. The glue applicator gun (used epoxy: *Araldite 2011*) is prepared and a new tip is installed. Approximately 5 ml of glue is a good amount. It is spread very thin on the plastic foil over the gluing table. The roller is then used to apply glue uniformly and smoothly over the whole frame safe the cross (f). A scalpel blade is moved over the frame faces to remove excessive glue. The scalpel is cleaned with a lint-free cloth. The

scalpel is also moved over the frame edges (g) and the corner hole edges to minimize glue on GEM areas that are not connected to the frame. Finally, a cloth impregnated with isopropanol is used to remove glue on the cross. Afterwards, the polymer frame can be moved back to the gluing jig and is inserted and pushed gently into the notch (h). Any glue on the gluing jig or on the gloves should be removed immediately with a cloth and isopropanol.

**Gluing.** The polymer frame's correct fit is again checked by inserting the metal pins into the four corner holes and removing them. The 'VectorGuard' frame with the stretched GEM foil is placed on top of the gluing jig. The polymer frame and the GEM are at a distance of approximately 0.5 mm. The 'VectorGuard's spring fasteners are closed. The frame-foil alignment is again checked using the microscope. The alignment should be unchanged due to the adjustment with the screws. The metal pins are inserted into the corner hole (i) and the cover plate (j) is mounted on top of the gluing jig (k). Pressure is applied by putting steel bricks on the cover. A hygrometer is placed in the middle of the cover plate. The whole system is covered with the transparent hood (l). The hood is flushed with nitrogen and the glue is left to dry for 24 hours. The gluing tools are cleaned with isopropanol. The applicator gun is turned off and the gluing tip is removed. After about 2 hours it is checked that a relative humidity of about 0% is reached.

**Retrieving the framed foil.** After 24 hours of glue drying, the nitrogen supply can be removed. The transparent hood is lifted and moved to its storage location. The hygrometer and the steel stones are carefully removed and the cover plate is lifted. The corner pins are removed. The 'VectorGuard' frame is connected to compressed air and supplied with a pressure of 5 bar in order to release the 'OptiGuard' frame. The GEM is lifted carefully. The proper gluing should be checked optically. The GEM is placed in the paper bag and stored in the dry cabinet. The next foil can be framed. If this is the last foil, gluing jig and 'VectorGuard' frame are put to their storage location.

## 4 Analytical approach to the leakage current test

A high standard in GEM quality is crucial in order to ensure the correct operation of the TPCU. Hence, the two main steps of quality assurance, the optical measurement and the leakage current test have to be well-understood and their informative value assessed. The focus of this thesis is the leakage current testing procedure (introduced in Chapter 3.2). This chapter aims at a better understanding of the test results: It is essential to recognize the determining factors for leakage current and how the testing conditions, e. g. gas humidity, can affect the measurements. Finally, by showing the test reproducibility not only the test quality is proven but also the appropriateness of the foils' storing conditions. This chapter is structured such that first, a general overview of the leakage current measurement is given and then, a number of hypotheses are tested.

### 4.1 Leakage current measurement results

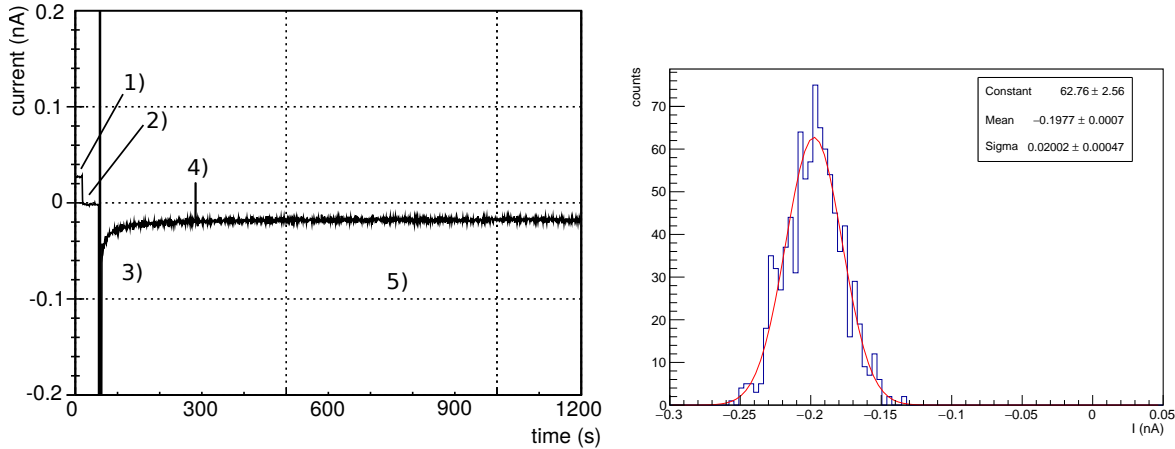


**Figure 19:** Left: The leakage current of one segment as a function of time during one measurement. The numbers correspond to the events explained in the text. Right: Histogram of the measured leakage current values for  $t \geq 300$  s. A Gaussian fit is applied. Mean and error of the mean are used as the quality evaluation of the foil. Used foil in both plots: OROC 3, GEM 4, number 004, segment 10.

Figure 19 (left) shows the time development of a leakage current measurement for one segment of an OROC3 foil. The underlying data is one leakage current value per second (per segment) for a duration of 1200 s; the values are obtained by the picoammeter as described in 3.2.2. There are several important steps marked in the plot which are explained in the following:

**1) The offset reference measurement.** To ensure that the measurement is as accurate as possible, it has to be freed from any constant offsets caused by the electronics. Therefore, the average current of 2 seconds<sup>10</sup> with no voltage<sup>11</sup> is taken and subtracted from

<sup>10</sup>empirical value

<sup>11</sup>The minimal output of the HV source is actually not zero, but  $U = 2.41$  V.

all ensuing measurement values. It has to be checked whether the offset was correctly taken; even small environmental changes such as human movements near the test box can induce currents in the GEMs on the scale of several 10 pA and distort the offset value. In the case shown in Figure 19 (left), the measurement has to be corrected for an offset of approximately 25 pA.

**2) Offset correction and voltage ramping.** The offset is measured and subtracted. The measurement continues at the same voltage for a few seconds in order to check that it has been done correctly. Also, the voltage is ramped to  $U = 500\text{ V}$  while the connection to the HV source is interrupted.<sup>12</sup>

**3) Foil charging.** When the HV source is reconnected to the GEMs, the foils are charged like a capacitor. In the plot, this corresponds to a high spike that decays exponentially with time, converging towards the average leakage current. The charging currents can reach several hundred nanoamperes and often reduce the voltage of the source due to its maximal power output. During the first approximately 300 s, the charging currents are too large to measure the leakage current.

**4) Discharge.** Due to the high voltage difference between the foil sides, discharges (often referred to as *sparks*) can occur. They happen for different reasons: Gas humidity, dust on the foils and defects in the GEM structure are some of them. They pose the risk of foil damage but luckily are rare, assuming good treatment of the foil. For illustration purposes, a measurement with a (yet small) discharge was chosen.

**5) High voltage leakage current measurement.** When the foil is fully charged, the leakage current is measured for about 900 s in order to obtain a representative measurement of the foil's behavior under high voltage. The duration of measurements depends on their goal. If the long-time performance of GEMs shall be evaluated, the measurements can last up to 12 hours. For getting a reliable leakage current value, 20 minutes per GEM is considered enough.

In order to assess the foil quality it is not necessary to look at the entire current-time development; in many cases, the relevant information can be expressed by a few numbers. In particular, if the foil performs well in the sense of no or only little discharges, it should be enough to characterize the foil quality with the performance of the segment's average and largest leakage current values. The leakage current measurement of one segment can be transformed into a single value as shown in Figure 19 (right): All measured values after foil charging, i. e. for  $t \geq 300\text{ s}$ , are plotted in a histogram. Under the assumption of a white noise distribution of the leakage current, the histogram is fitted with a Gaussian. The fit's mean value  $I = (-18.1 \pm 0.1)\text{ pA}$ <sup>13</sup> gives the best approximation of the leakage current of this segment. The standard deviation  $\sigma$  has been found to vary with the foil but also with different measurements of the same foil; it is possible that there is a source

---

<sup>12</sup>Voltage ramping of GEM foils is in general safer when arriving at the target voltage as fast as possible. Slow ramping might cause melting of any potential dust on the foil, while fast ramping is believed to burn the foil clean. By disconnecting the HV source before ramping and connecting it afterwards, the fastest ramping is achieved.

<sup>13</sup>The picoammeter's manufacturer specifies its measurement error at 23 °C and a measurement accuracy of 0.1 pA to 0.2 %.

of electromagnetic noise in GSI’s clean room, however, the source could not be identified. Fortunately, it does not have an effect on the mean value. For the following examinations we will thus work with the mean and its error given by the Gauss fit.

## 4.2 The area dependence of the leakage current

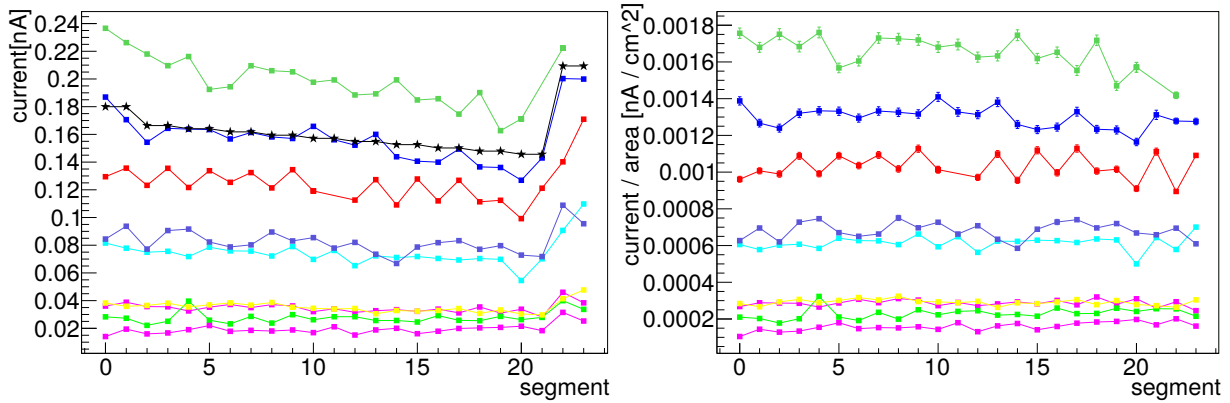


**Figure 20:** Left: The absolute leakage currents per segment for nine OROC3 foils (squares). The error bars are too small to be displayed. The current values of the same foil are shown in the same color and connected by lines. Marked with a black star is a scaled version of the area of each segment. A proportionality between area and leakage current is visible, especially when comparing segment 22 and 23 to the rest. Right: When dividing the same leakage current values by the area of the respective segment, the values per measurement converge to a similar level.

Multiple leakage current tests are an integral part of the processing of each GEM foil. In tests on the pre-production foils it was found that for OROC 3 foils the leakage currents of the last two segments are systematically higher than the currents of other segments. One possible explanation referred to possible inhomogeneities during the etching process, another simply to the area differences of the segments. The latter can be explained like this: A higher number of foil holes means more possibility for electrons to pass from one foil side to the other. To analyze the effect, nine measurements of OROC3 GEMs are plotted in Figure 20 (left) with square markers. The measurements are chosen because they were taken under comparable conditions: All GEMs were measured shortly one after another within the duration of two days and they went as a batch through the same working process.<sup>14</sup>

When comparing different GEMs in order to see a difference in pitch size, one has to bear in mind that the decoupling resistors<sup>15</sup> vary in resistance: In GEM 1, 2 and 3 the resistance value is  $R_D = 5 \text{ M}\Omega$ , but GEM 4’s resistor has a value of  $R_D = 1 \text{ M}\Omega$ . However,

<sup>14</sup>All foils were produced at CERN, then shipped to the *Helsinki Institute of Physics* for optical quality assurance and finally shipped to GSI.

<sup>15</sup>Each segment is connected with the HV supply path via a decoupling resistor. For details, see Chapter 2.2.

this difference can be corrected with a simple calculation. A look back on the wiring diagram in Figure 12 is helpful: The leakage current of a single GEM segment  $I_L$  is split in a parallel connection between the decoupling resistor  $R_D$  and the protection resistor for the ampere meter  $R_A = 10 \text{ M}\Omega$ . The current measured by the ampere meter  $I_A$  is given by

$$I_A = \frac{R_D}{R_A + R_D} \cdot I_L \quad (1)$$

As a consequence, the measured current is lower by a factor 3 compared to the leakage current for GEM 1-3 and lower by a factor 11 for GEM 4. It can be corrected by multiplying with the respective factor.

The curves in Figure 20 (left) vary by more than one order of magnitude, between 10 and 240 pA and well below the specification  $I_{L,\text{max}} = 500 \text{ pA}$ . Moreover, most of the segments show little variation *within* the same measurement. This is an expected behavior as etching and hole properties should have little variance within one foil and environmental conditions such as air humidity are equal for the segments. Nonetheless, a slight negative slope in the curves is visible and furthermore, the first two segments have slightly and the last two segments strongly increased current values. It will be shown that this effect can be explained by the area differences of the segments.

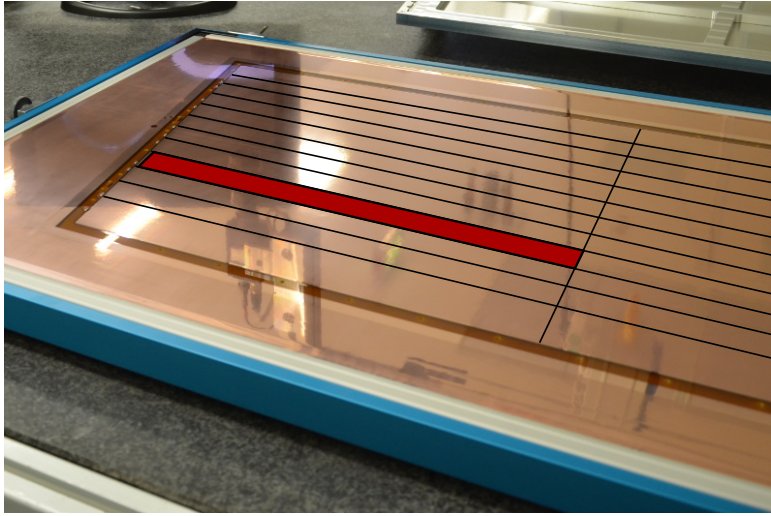
Even though the area was intended to be about  $100 \text{ cm}^2$  for each segment (see Chapter 2.2), due to the layout decision the areas actually deviate strongly. For the purpose of this study the areas of the segments are remeasured. As *segment area* is considered the ‘active area’, the part of the GEM foil that is perforated, which excludes approximately 1 mm on each border (Figure 21 (left)). Because of this exclusion the sum of all the segments is slightly smaller than the value given in the TPCU Technical Design Report (TDR)<sup>16</sup>. The results can be found in Figure 21 (right). The photo also illustrates the reason for area differences: The designers chose to give all segments except for the top and bottom ones the same height (30 mm). This circumstance together with the trapezoidal shape of the GEMs lead to the area differences.

As it stands out from the table, the area of the segments decreases with increasing segment number save the first and last segments. The largest segment is 44% larger than the smallest segment (segment 21 versus segment 22). This indeed can explain the rise in the last segments. To visualize the effect, the leakage current values divided by the area of the respective segments are plotted against the segment number (Figure 20 (right)). The slopes within the same measurements are reduced and the deviations of the first and last segments vanish. The plot provides an indirect indication on the leakage-current-area dependence.

In order to see a direct proof, the leakage current values are plotted as a function of the area of their respective segment. The result is the correlation plot in Figure 22; the underlying data is the same as before. The individual foils can be distinguished by the marker color. There are two current values on the same area for each measurement because

---

<sup>16</sup>For OROC3  $A_{TDR} = 2949.0 \text{ cm}^2$  [3]



Segment	area [cm <sup>2</sup> ]
0, 1	134.7 ± 2.1
2, 3	124.5 ± 2.1
4, 5	122.8 ± 2.0
6, 7	121.1 ± 2.0
8, 9	119.3 ± 2.0
10, 11	117.6 ± 2.0
12, 13	115.9 ± 1.9
14, 15	114.2 ± 1.9
16, 17	112.4 ± 1.9
18, 19	110.7 ± 1.8
20, 21	109.0 ± 1.8
22, 23	156.7 ± 1.8
Σ	2918 ± 7

**Figure 21:** Left: Illustration of the GEM segmentation. Marked with red is the area of one segment. Right: Measured OROC3 area values. Due to the symmetry of the foil, two subsequent segment sizes are identical.

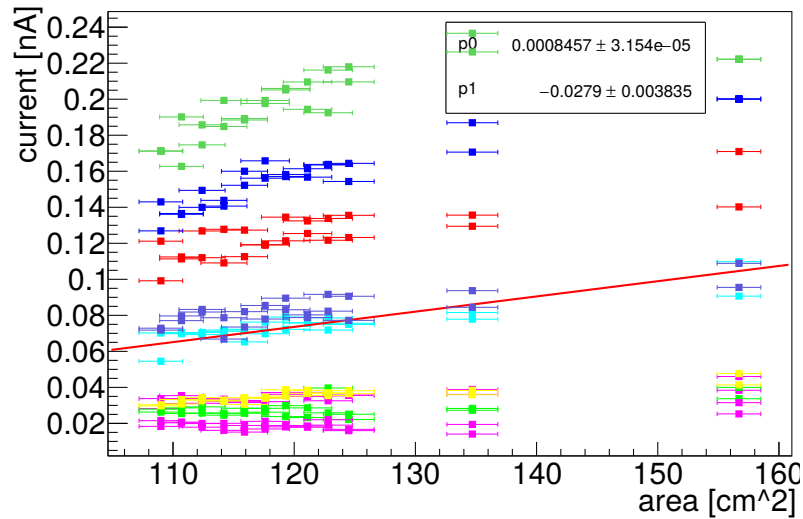


**Figure 22:** Segment leakage current as a function of segment area for nine OROC3 GEMs. Foils can be distinguished by marker color. Points are omitted when the offset in the measurement was not correctly taken. A linear fit is applied to the turquoise values.

No	GEM	$p_0$ [ $10^{-5}$ nA cm $^{-2}$ ]	$p_1$ [ $10^{-3}$ nA]
1	1	$85 \pm 3$	$-28 \pm 4$
2	1	$130 \pm 5$	$-33 \pm 6$
3	2	$33 \pm 2$	$-12 \pm 3$
4	2	$30 \pm 2$	$-1 \pm 3$
5	3	$26 \pm 2$	$3 \pm 2$
6	3	$17 \pm 2$	$-2 \pm 3$
7	4	$180 \pm 7$	$-20 \pm 8$
8	4	$79 \pm 3$	$-13 \pm 4$
9	4	$153 \pm 5$	$-29 \pm 6$

**Figure 23:** Results for linear fits  $I = p_0 \cdot a + p_1$  applied to the individual measurements like for turquoise in Figure 22 (left).

the area of two subsequent segments is the same. Looking at only one measurement one can see that the leakage current rises with the area. To illustrate this, a linear fit is applied to the turquoise measurement. The parameters given in the box are for the formula  $I = p_0 \cdot a + p_1$ . The parameter  $p_0$  can be interpreted as a factor that quantifies how the leakage current rises with the area. Interestingly, the second parameter  $p_1$  does not incorporate 0 pA in its  $3\sigma$  error bounds as expected: At vanishingly small area the leakage current should also vanish. It could be an indication that the functional dependence is of a higher order than expected. However, given only little measurement data, a higher order fit seems not meaningful.

Instead, a linear fit is applied to every measurement individually and the parameters are compared in the table in Figure 23. It is interesting to see that the fit values for  $p_0$  show a certain pattern: Three out of the four values for GEM 2 and GEM 3 share a  $2\sigma$  error range for  $p_0 = 30 \cdot 10^{-5}$  nA cm $^{-2}$ . For GEM 1 and 4 only two out of five share a  $2\sigma$  range, the rest deviates significantly but is all above  $79 \cdot 10^{-5}$  nA cm $^{-2}$ . The difference that appears in the table can be explained with the GEM's pitch sizes, as is explained in the next chapter.

The conclusion to be drawn from this chapter is that the leakage currents of different segments can only be compared when normalizing by the area. The same has to be done when comparing whole foil's leakage currents.<sup>17</sup> It results the consequence that the characterization of a single foil by their segments' average and segments' largest leakage current, as it is proposed in Chapter 4.1 and as it is recommended practices in the TPCU database, is based on the wrong assumption of comparability of the segments. For instance, this would lead to the fact that the segment with highest leakage current is in most cases segment 22 or 23, but only because of a bias. A better characterization would be derived of the comparable quantity leakage current divided by area. From this, the average and the largest value can be taken for foil characterization.

<sup>17</sup>From the TPCU TDR it can be seen that there is a factor of about 50% between OROC1 ( $A_{TDR} = 1997.3$  cm $^2$ ) and OROC3 foils ( $A_{TDR} = 2949.0$  cm $^2$ ).

### 4.3 The pitch size dependence of the leakage current

In the last chapter, it is found that the leakage current shows a dependence on the GEM's area. A simple physical explanation behind the dependence is that each hole provides a possibility for electron passage; the more holes there are, the more leakage current flows.<sup>18</sup> It was also seen, that the slope for the leakage current's rise with increasing area can be partly explained with the pitch size. In this chapter, it will be examined if the pitch size is also a good predictor for the individual leakage currents of the foil.

As previously mentioned, GEMs differ in pitch size. More precisely, there are two categories of GEMs: GEM 1 and GEM 4 foils have the 'standard' pitch size of 140  $\mu\text{m}$ , whereas GEM 2 and GEM 3 have the 'large' pitch size of 280  $\mu\text{m}$ . Assuming a proportionality between leakage current and number of holes, the change in leakage current can be predicted with the help of Figure 24 (left). As a result of the hexagonal hole arrangement, a doubling of the pitch size causes a decrease in the number of holes by a factor of approximately 3.46. Hence, the 'standard' pitch size GEMs should be subject to 3.46 times higher leakage current than the 'large' pitch size GEMs, assuming that other determining factors such as hole size are equal.

As observable in Figure 20 (left), the leakage currents take values that vary between 10 and 240 pA even in comparable measurements. This cannot be explained with the expected factor of 3.46 for the pitch size dependence alone. It is an indication that there are further determining factors for a foil's leakage current which superimpose the pitch size. To observe the dependence, one has to take either a big amount of data and prove it in form of a correlation plot or compare measurements of the best-performing foils. The latter works with the assumption that ideal foils have a clear defined leakage current (an upper limit) and that higher leakage currents arise due to flaws in the GEM structure. By taking the foils with smallest leakage current, the upper limit might be found and it might reflect the pitch size dependence.

Collecting a big amount of comparable data is an inapproachable option by the means of this thesis. Working with existing measurement data from all institutes has the complication that in spite of all efforts to standardize the testing procedure, the measurements from different institutes are still not comparable. On that account, the second strategy is followed. However, it has to be kept in mind that every measurement poses a risk to the foils; thus, the measurement of the best-performing foils is not an option as they are the best candidates for integration in the TPCU. Instead, the comparison measurements are conducted on a set of redundant foils. From this set, the best candidate of GEM 1, 2 and 4 is chosen in terms of lowest average leakage current (area normalized) in past measurements.

All beforehand considerations result in the following measurement procedure: The measurements are taken on three selected, well-performing foils of GEM 1, 2 and 4. Each

---

<sup>18</sup>There are other determining factors, for instance the hole size is correlated with the leakage current. Even though the outer diameter of every hole should be 70  $\mu\text{m}$ , there are fluctuations over all foils and even within the same foil.

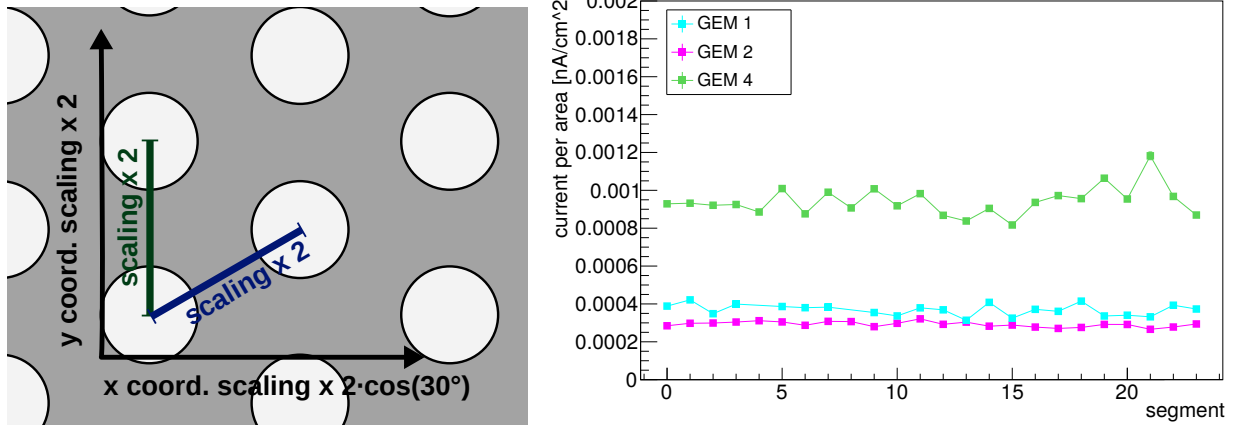


**Figure 24:** Left: Sketch to illustrate the relationship between number of holes and pitch size. By doubling the pitch size, the number of holes per area decreases by a factor of  $2 \cdot 2 \cos(30^\circ) \approx 3.46$ . Right: Comparison of three measurements for three different GEMs. GEM 2 and GEM 3 are identical in pitch size and decoupling resistor; thus only GEM 2 is measured. Two points of the GEM 1 measurement are omitted because of a connection defect in the test box.

of them represent a different configuration in terms of pitch size and decoupling resistor. The measurement is conducted in a brief period of time to ensure the comparability of the measurement conditions.

The results of the measurements are shown in Figure 24 (right). The leakage currents normalized by the area are plotted as a function of the segment number. Each individual measurement is drawn in a different color and the measurement points are connected by lines. Within the measurements, the segments only show little relative deviation. Comparing the measurements, the expected effects cannot be seen: The segments of GEM 1 and 4 are expected on a comparable level but in fact, the tested GEM 4 foil has a higher leakage current by a factor of approximately 3. On the other hand, GEM 1 and 2 only show relative differences between 1.05 and 1.45; expected was a difference of the factor 3.46 due to the pitch size. Apparently, other factors outweigh the pitch size in this particular case. These could be intrinsic foil properties, such as the hole diameter or the amount of structural imperfections.

However, the pitch size is observed in the last chapter: In Figure 22 and the table in Figure 23, there was visible discrepancy in the slope for the area dependence of the ‘standard’ and the ‘large’ pitch GEMs. Three out of the four values for GEM 2 and GEM 3 share a  $2\sigma$  error range for  $p_0 = 30 \cdot 10^{-5} \text{ nA cm}^{-2}$ , while all GEM 1 and GEM 4 values are above  $79 \cdot 10^{-5} \text{ nA cm}^{-2}$ . This can be explained with the pitch size, as the hole number increases stronger with the area when the hole density is higher. One expects the same factor of 3.46 between the different pitch sizes, so from the best-guess for the GEM 2 and 3 slope  $p_0 = (30 \pm 2) \cdot 10^{-5} \text{ nA cm}^{-2}$  one would expect a GEM 1 and 4 slope of  $p_0 = (104 \pm 7) \cdot 10^{-5} \text{ nA cm}^{-2}$ . The value deviates significantly from all slopes obtained for GEM 1 and 4, nevertheless, the change in pitch size seems to explain at least partly the differences in the slopes. Other factors seem to further alter the slopes, among them

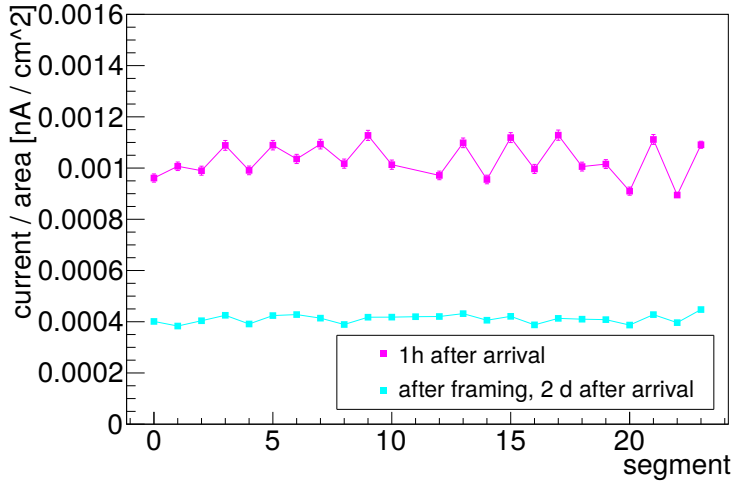


**Figure 25:** The area-normalized leakage current of a foil as a function of segment number. The same foil shows a different average by a factor of about 2.5 when comparing the time steps 1 hour after arrival and 2 days later. This is an indication that the foils’ quality is short-time affected by the shipping process. One has to bear in mind, however, that the foil is framed between the two steps, even though it seems unlikely that this increases the foil quality.

might be a fluctuation in hole diameter.

The offsets  $p_1$  also show a certain pattern with respect to ‘standard’ and ‘large’ pitch, however, it is not as clear as the slope pattern. Three of the four values for GEM 2 and 3 have 0 nA in their  $3\sigma$  error range which fits well to the expectation: As aforementioned, for a vanishing area size the measured leakage current should vanish, too. Of the GEM 1 and 4 values, only measurement 7 has 0 nA in its  $3\sigma$  error range, the others deviate significantly. A possible explanation for this deviation could be the non-linear effects that increase with higher leakage current: The leakage current values for GEM1 and 4 are the highest five in Figure 22. Looking at the highest measurement (green), a non-linear effect seems possible.

The conclusion to be drawn from the results is that the pitch size has an observable effect on the leakage current. However, in a particular measurement, it may be outweighed by other factors. Among those factors may be gas humidity, imperfections in the GEM structures or noise sources in the lab.

#### 4.4 The foil humidity dependence of the leakage current

The GEM foils are always treated with extraordinary care and strong limitations on the environmental conditions. In the clean room, the environmental conditions can be easily controlled: The relative air humidity (RH), the ratio of partial pressure of water pressure to equilibrium water vapor pressure, is kept at a level of 20 % and a temperature of 23 °C is maintained. Nevertheless, it is interesting to know how sensible are the foils to their environmental conditions. During the shipping of the foils these conditions are possibly

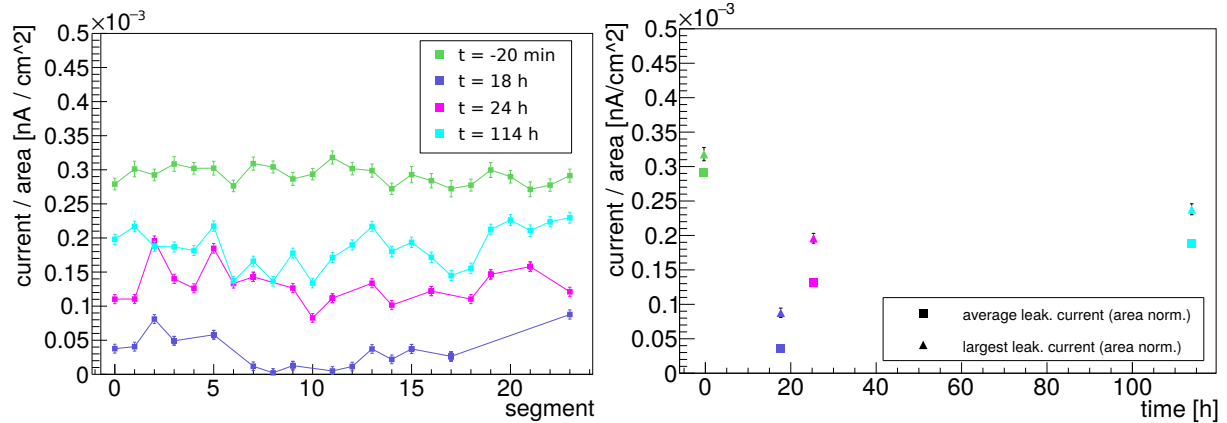


**Figure 26:** Left: Area normalized leakage current of four measurements of the same foil that is exposed to 20 % RH. Each measurement is drawn with a different color and connected by lines. The colors correspond to the colors in the right plot. Points are omitted when their value is so low that the ampere meter’s accuracy is not sufficient. Right: The average and maximum value of each measurement are taken and plotted as a function of time. At  $t = 0$  h, the GEM foil is exposed to the 20 % RH conditions of the clean room. The first measurement ( $t = -20$  min) is taken on the dry foil for comparability.

not maintained because the transportation box is equipped with a membrane in order to achieve an equilibrium with the outside air pressure. This might lead to high levels of air humidity inside the transport box. It is imaginable that this influences the foils on a longer timescale: The small holes in the GEM foils might act as capillaries and accumulate water. This in turn might enlarge the leakage currents, when not reversed by storing the foils in an environment of low air humidity (e.g. the dry cabinet with 0 % RH). An indication for this effect is given in Figure 25: The measurement in purple is taken only about an hour after the arrival of a foil from shipping. It shows highly increased values with a strong variation in the segments. This behavior, however, vanishes in a second measurement on the same foil taken 2 days later and after the framing. It cannot be ruled out, but it is considered unlikely that the framing process enhanced the foil quality.

An obvious way to inspect this effect is to take a foil and measure the leakage current before, during and after the exposition to a high-humidity environment. A controlled and clean environment with a high air humidity is unfortunately not available. Instead, the clean room with its relative air humidity of 20 % can be used. This cannot answer the question about the impact of normal outside air humidities on the GEM foils. It can, however, give an indication about the correct treatment of the foils in the clean room: During the foil processing, in particular when soldering resistors to the foils, it can happen that a GEM foil stays up to three days in the clean room, not in the dry cabinet as usually. It is interesting to see whether this has an impact on the performance of a foil in terms of the leakage current.

In order to answer this question, the following experiment was designed: A well-performing foil is measured, then stored in the test box but exposed to clean room air of 20 % humidity, which is checked with the hygrometer. It is measured again after 18, 24 and 114 hours.

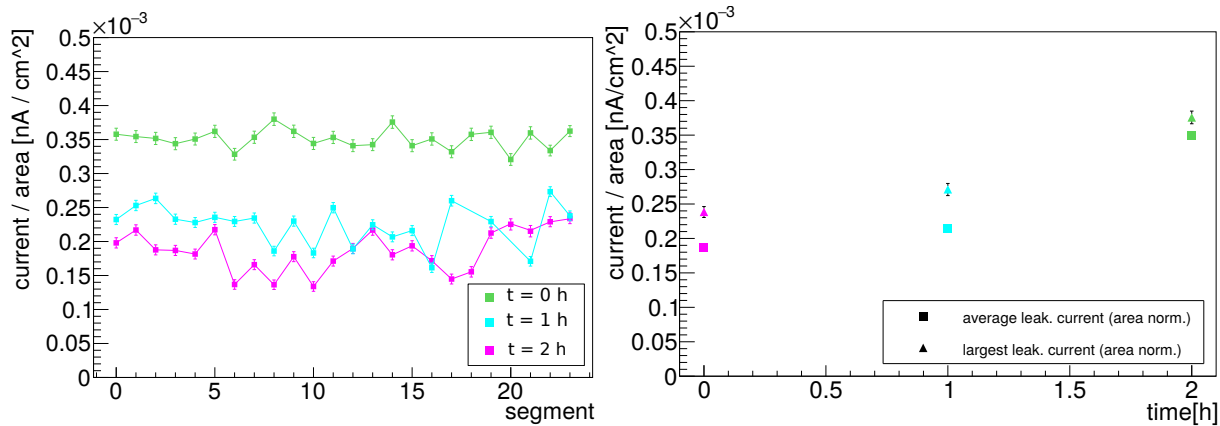


**Figure 27:** Left: Area normalized leakage current of three measurements of the same foil that was exposed to 20 % relative humidity and is in this plot stored under 0 % RH conditions. Each measurement is drawn with a different color and connected by lines. The colors correspond to the right plot. Points are omitted when their offset was not determined correctly. Right: The average and maximum value of each measurement are taken and plotted as a function of time. At  $t = 0$  h, the GEM foil is exposed to the 0 % RH conditions of the test box flushed with nitrogen.

To determine how long an effect lasts, the foils are then stored at 0 % RH conditions and measured again after 1 hour and 2 hours. One has to keep in mind the limitations of this procedure: The measurement prescription foresees that the foil is exposed to about 30 minutes at dry gas conditions.<sup>19</sup> If the drying effect of the foil is as fast as 15 minutes, it is probable that there is never any effect observed. If the drying effect is faster than 30 minutes, than each measurement resets the time spent in humid conditions to zero; yet this should be evident from the results.

Figure 26 shows the results of the humidity exposition. The left plot gives the details of the measurements in an area-normalized leakage current per segment plot. It is visible that the measurements show different levels of leakage current, as expected. An interesting detail is that the relative values are not maintained: A segment can be the highest in one measurement and the lowest in another. As discussed in Chapter 4.1 each measurement can be summarized by the characteristic average and largest leakage current values. This is used in the right plot: The characteristic values are plotted as a function of time. At  $t = 0$  h the foil is exposed to 20 % relative humidity conditions; the first measurement is taken shortly before at  $t = -20$  min. The results, however, are surprising: The highest leakage currents flow before the foil is even exposed to humidity conditions. After 18 hours of humidity exposition the average leakage current shrinks by a factor of approximately 6. With further increasing time a rising trend can be observed, nevertheless, the highest leakage current reached after 114 hours is still lower than the one of the dry foil. An explanation of these results could be that the first measurement is influenced by some yet undetermined factor to produce higher results. This is, however, not the full explanation

<sup>19</sup>The test box has to be flushed with nitrogen until the gas humidity is below 10% for about 10 minutes and the measurement takes additional 20 minutes.

which becomes clear when looking at the next set of measurements.

After 114 hours of humid air exposition, the foil is exposed to dry air conditions. This is achieved by putting it into the test box which is flushed with nitrogen. It is then measured directly, after 1 and 2 hours. The results are shown in Figure 27. The measurement at  $t = 0$  h is the same as the measurements at  $t = 114$  h in Figure 26. In the left plot, it can be observed that the leakage current is at different levels for the measurements. It does not maintain a relative structure of the segments; the values are not simply shifted but show distinct behavior in each measurement. The time development of the average and largest leakage current in the right plot yields further unexpected results: The longer the GEM foil stays in drying conditions, the higher leakage currents are obtained. These results are opposite to the prediction.

Even though the measurement data seems to suggest that the GEM foils perform better after being exposed to slightly humid conditions, this hypothesis comes out to be implausible. The TPCU group at the University of Bonn showed consistently and with more ground data that the leakage current of a foil has a strong non-linear dependence under gas humidity conditions above 40% relative humidity. This, however, refers to gas humidity during the measurement, not to a long-term foil exposition to gas of that humidity. Hence, it is possible that the relative humidity of 20% in the clean room is not high enough to have a visible effect. In this case, the question remains why the values show such a high fluctuation. Another interpretation of the results is that there is at least one other factor that dominates the average level of the leakage distribution. It can only be guessed what this factor is; a charging effect of the test box might explain the rising trend seen in Figure 27 or a general source of noise in the clean room may influence all measurement, unfortunately, this can not be investigated in the scope of this thesis.

The conclusion of this chapter is that quantitative values of the leakage current measurement may be not as reliable as expected. Thus, the next step will be a test of the reproducibility of the measurement results.

## 4.5 Reproducibility of measurements

The beforehand experiments are all conducted on the premise of reproducibility of the leakage current measurement. However, this is not necessarily true and has to be verified, particularly with regard to the results obtained in the last chapter. The significance of reproducibility is high: If multiple measurements of the same foil do not yield comparable results it is hard arguing that the leakage current measurement is reliable on a quantitative level.

There were slight indications that reproducibility might not be given: During the analysis of the pre-production foils, different measurements of the same foil showed not only varying amounts of leakage current, but also differences in the signal's noisiness (the standard deviation in Figure 19, right). The suspicion arose that there was a source of electromagnetic noise in the GSI's clean room which might be more or less active on different days. In the same context it is noticeable that the leakage current tests conducted at CERN

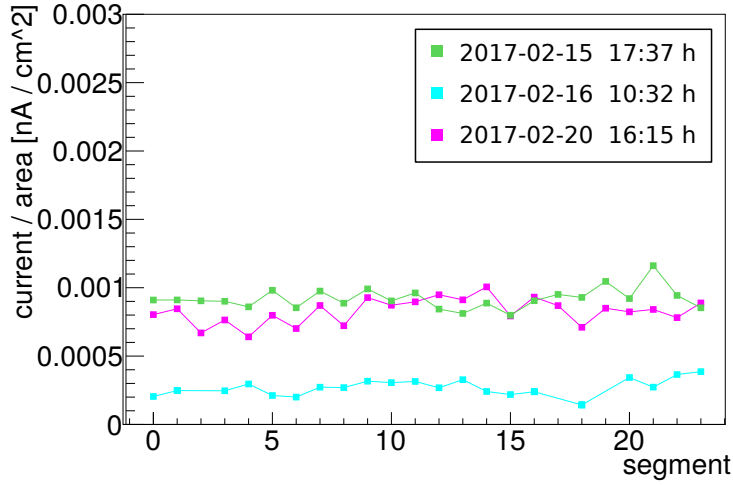


**Figure 28:** The area-normalized leakage current as a function of segment number. Three different measurements of the same foil are shown. The measurements have the following average values: purple  $(827 \pm 3) \cdot 10^{-6} \text{ nA/cm}^2$ , green  $(924 \pm 3) \cdot 10^{-6} \text{ nA/cm}^2$  and turquoise  $(278 \pm 2) \cdot 10^{-6} \text{ nA/cm}^2$ . The average values are determined by dividing the sum of all segments by the total area. None of them coincide in their  $3\sigma$  error range, nevertheless, the difference between purple and green is small compared the difference between purple and turquoise.

often show a smaller standard deviation. On the other hand, the results obtained so far are based on the mean – noise might only have an impact on the standard deviation. To shed light on this theoretic considerations, the reproducibility shall now be examined practically.

The aforementioned considerations lead to the construction of the following experiment: An existing foil is selected that has proven to perform well. It is measured four times, on four different days and on four different times of the day. The measurement procedure is the same every time: The GEM is taken out of the dry cabinet and put into the test box. The test box is flushed with gas for approximately 10 minutes, then the leakage current is measured and the foil is brought back into the dry cabinet for storage. In a positive test outcome, not only the reproducibility of the test is shown but also the appropriateness of the foils’ storing conditions in the dry cabinet.

The plot in Figure 28 presents the results of the conducted experiment. Only three of four planned measurements are shown; in the fourth and last measurement, the foil unfortunately developed a short circuit and the data cannot be used. As evident in the plot, all measurements significantly differ in their average value. The green measurement’s average is about 11% higher than the purple one, so the two can be considered as comparable. The purple measurement, however, shows values approximately 3 times higher than the turquoise measurement. This is a noticeable difference.

A few short calculations help to get a better feeling for the discrepancy between the measurements: The absolute difference between purple and turquoise is  $(549 \pm 2) \cdot 10^{-6} \text{ nA/cm}^2$ . By multiplying the value with the average area of a segment  $A_{\text{avg}} = (121 \pm 7) \text{ cm}^2$ , one gets

an approximation for the average difference in leakage current between the two measurements:  $\Delta I = 66 \pm 3$  pA. With Equation 1, one can calculate the corresponding measured current by the picoammeter of  $I_A = (6.0 \pm 0.3)$  pA. The same calculations for the green and turquoise measurements lead to the following values:  $\Delta I = 12 \pm 1$ ,  $I_A = 1.1 \pm 0.1$  pA<sup>20</sup>.

From the results obtained in this experiment it is evident that the measured leakage current can fluctuate up to 60 pA. An important question is whether this is an upper limit on the fluctuation in the sense that that the measurement is reproducible with a maximal error of  $\pm 60$  pA. Even though this means that the leakage current measurement is not as reliable as was thought, it would still provide enough accuracy to confirm that the leakage current of a segment is below 0.5 nA. The data presented in this thesis give no indication of a higher upper limit; the largest difference of two measurements of the same foil observed in other chapters was  $\Delta I = 31 \pm 2$  pA<sup>21</sup>.

Overall, the impact of the limited reproducibility is not expected to be fatal for the project due to a high production of spares: From experience, very few GEMs have an average leakage  $I_{\text{leak}} > 0.44$  nA, where the observed measurement uncertainties do not guarantee that we are below the specifications of  $I_{\text{leak}} < 0.5$  nA. For implementation in the TPC, the best foils according to their leakage current are selected, so the few critical foils would always be replaced by spares. Nevertheless, a larger series of measurements should be conducted to examine the effect and to make sure that the leakage current test is reliable. The foil analyzed in this chapter had a small average leakage current in comparison to other foils; it should be determined whether the variation of measurement results enlarges or shrinks with higher leakage currents.

All in all, there must be a yet undetermined factor that influences the measurements. An explanation could be that some part of the test setup serves as an antenna and receives electromagnetic waves and noise. This could be for instance the GEM itself or the pins that establish contact with the segments. It seems plausible that the setup is susceptible to induction effects: The measured currents on the picoammeter scale are extremely small and simply waving a hand 30 cm over the test box creates currents up to 100 pA. Yet it is not clear how this source of noise influences the leakage current's mean value; normal induction effects created by waves are expected to rather increase the variance. Finally, the data indicates that the foil's storage conditions are appropriate: After four days of storage in the clean room (between first and third measurement), the levels of leakage current are similar.

---

<sup>20</sup>The picoammeter's manufacturer specifies its measurement error at 23 °C and a measurement accuracy of 0.1 pA to 0.2%. The measured currents in this measurement had a mean of at most 10 pA which would result in a measurement error of 0.2 pA. This alone cannot explain the discrepancy.

<sup>21</sup>In Chapter 4.4, Figure 26 (left), the difference in average leakage current of the green and the blue measurement.

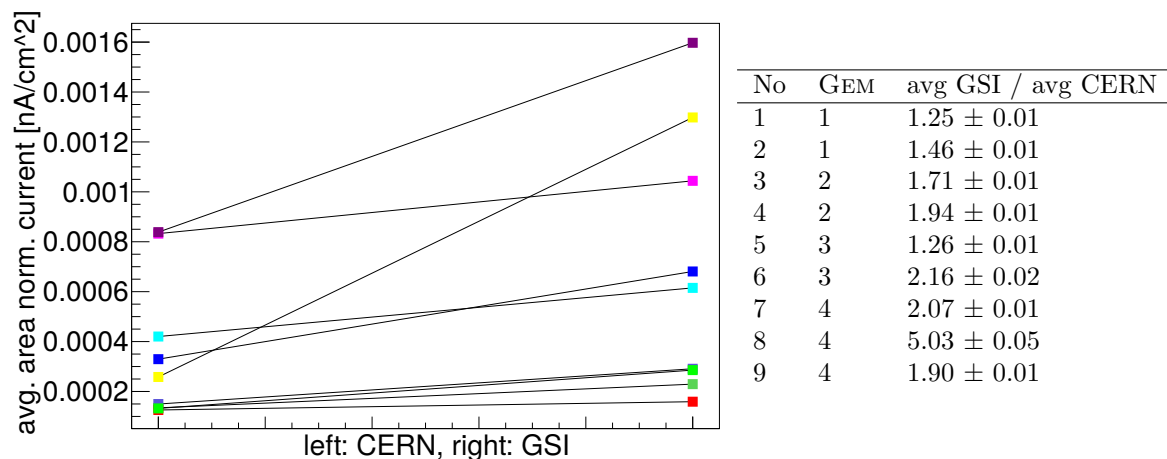


**Figure 29:** Left: Comparison between nine measurements for the same foils at CERN and GSI. Shown is the average leakage current per area. Right: The table lists the GEM number as well as the factor between average of the measurement conducted at GSI and CERN.

## 4.6 Data comparison with other institutes

The results obtained in the last chapter revealed that the reproducibility of measurements in the GSI’s test setup is limited. An important question at this point is whether this limitation is also present in the setups of other institutes, for instance at CERN. The only option for a direct proof is the conduction of the reproducibility test at these institutes. Unfortunately, this is not possible in the scope of this thesis. Nevertheless, a comparison between the measurement results of GSI and other institutes for the same foils can help to assess the disturbances encountered at GSI and provide an indication whether the intrinsic foil properties or the noise determine the measurement values.

The TPCU database lists detailed information for every processed foil, including all the data of leakage current measurements. The database’s information is used in the following in order to compare tests conducted at CERN and GSI. At least three assumptions are made when using the data for a comparison: First, the shipping has no impact on the foil performance, secondly, that the measurement results obtained at GSI are to some extent representative and thirdly, that the measurements at CERN are reproducible and characterize the foil’s properties. These assumptions have to be verified and are not necessarily true; especially the second one is threatened by the limited reproducibility.

The gathered data is for the same nine foils of one batch that is also used in Chapter 4.2. The respective average leakage currents per area of the same foils at CERN and GSI are plotted in Figure 29 (left). As observable in the plot, the relative spread of leakage currents is not only for GSI’s, but also for CERN’s measurements relatively large with a range from 0.15 to 0.85 pA/cm<sup>2</sup>; this encourages the theory that the measured leakage currents can mostly be explained with intrinsic foil properties. It is also visible that all leakage currents measured at GSI are higher compared to the values measured at CERN. As evident from the plot, the values’ relation between the institutes does not follow a

trivial behavior like an offset (can be seen from the two purple measurements) or a factor (can be seen from the different slopes). However, the ‘ranking’ of the foils seems to be maintained to some extent: The four foils with lowest leakage current at CERN stay the best foils at GSI and also three out of five of the foils with higher leakage current keep their ordering. A normalization of the values of GSI’s measurements by CERN’s measurement might reveal further correlation. The factors given in the table in Figure 29 (right) are obtained. The values are mostly in a range between 1.2 and 2.2 except for an outlier, measurement 8, with a factor around 5.

This fluctuation between 1.2 and 2.2 might be the best estimate for the noise we can get: Assuming that the CERN measurements provide a ‘true’ value for the characterization of the foils’ intrinsic properties and that the noise acts linearly on the CERN value, one could say that the noise adds an extra 20 % – 120 % of average leakage current to the foils. This would mean that the foil properties contribute between 45 % and 83 % to the value that the measurements at GSI yield; the rest is noise. However, this estimate has its limits with regard to the limited reproducibility found in the beforehand chapter. Remembering the found worst-case uncertainty of  $(66 \pm 3)$  pA for GSI’s measurements, the plot in Figure 29 (left) might change entirely if another set of measurements was taken.

## 5 Discussion

In this thesis, the leakage current tests for GEM foils are analyzed on a quantitative level; it is sought to examine the influence of various factors on the leakage current. It is shown that the leakage current depends on the *segment's area* and that relative differences between the segments in one measurement can partly be explained by the segments' different area sizes. An important lesson learned from this is that the quantitative comparison of currents from different segments makes no sense unless normalizing them by the segments' area. As a result, a suggestion arises for the further handling of foil comparison in the TPCU database, where the largest leakage current is the fundamental value for foil characterization: The segment that shows highest probability of breaking down in a high-radiation environment might not be the segment with highest leakage current (which is in most cases segment 22 or 23) but the one with highest leakage current per area, because it might have the highest amount of structural imperfections. If the value leakage current per area is found to be too abstract for intuitive characterization, the foil could still be characterized by the leakage current of the segment with highest leakage current per area.

Apart from the segment's relative deviations it was seen that different GEM foils can have entirely different levels of average leakage current. The *pitch size* is only partly able to explain these different leakage current levels. As shown, two foils with different pitch sizes can have a comparable average leakage current because it can be outweighed by other factors. Nevertheless, the difference in pitch size could be observed in the dependence of leakage current with the area: It was found that the leakage currents increases stronger with the area when the pitch size is smaller.

At this point, it shall be reminded of the statistical limitations of the presented measurements. As pointed out, it was not possible to acquire as much data as desired. Furthermore, it has to be also understood that the usage of all segments might not increase the statistical significance, since the segments are statistically correlated. This can be seen clearly from Figure 20: Leakage currents of different segments within the same foil are always on a similar level for all segments. These limitations have to be kept in mind, however, they do not alter the nature of the findings.

Further investigation lead to the question whether the leakage current depends on the storage conditions of the foil, in particular if a storage for multiple days in the (relatively) humid clean room has a negative effect on the leakage current. The data presented can be interpreted such that the opposite is true, namely that the performance of a foil improves after being exposed to 20 % RH conditions and that it changes for the worse when drying the foil. Another interpretation of the results is that the influence of 20 % is comparably small to other effects determining the leakage current.

Observing these results it is understandable to question the storage necessity of the foils in the dedicated dry cabinets: If the 0 % RH environment does not clearly improve the leakage current compared to the clean room, what is the point of this additional effort? There are three important aspects to discuss in order to approach this question. First,

the advantages of a dedicated storing place for GEM foils should not be underrated. A shielded location protects the foils from other influences in the clean room such as dust, humidity and electrostatics. The second argument is of statistical nature: Even though the influence of dry environmental conditions might not necessarily be visible at each foil, there can still be a correlation for a larger amount of data. Lastly, the GEMs have shown to be highly susceptible objects. During the measurements of this thesis, one well-performing foil developed a short circuit despite all caution and good treatment. Thus, the argument of highest feasible precaution seems sensible.

It becomes more evident that there are still undetermined environmental influences on the leakage current when one particular foil is tested in multiple measurements in order to show reproducibility. It was well-known that GEM foils are elaborate objects with a complicated production process and that they are subject to imperfections, e. g. in their hole structure. It was also well-known that GEMs are very susceptible towards environmental conditions, however, it was still a fundamental premise of beforehand measurements that the environmental conditions and other sources of disturbance and noise are sufficiently under control to reproduce measurements. This could not be confirmed; in just three measurements, one deviated from the others by about 60 pA in segment's average. This actually serves to understand better the unexpected results for the pitch size measurement and the gas humidity storage conditions analysis. It is nevertheless desirable to find the sources of yet unexplainable effects. A few possible objects of future investigation shall be detailed here:

**Antenna effect.** Relatively little effort is needed to induce a current into the GEM: The simple waving of a hand over the GEM area induces a current that gives short-term peaks of up to 100 pA. Thus, it seems plausible that GEMs also act as antennas for electromagnetic noise and maybe even radio waves<sup>22</sup>. A solution to this would be the shielding of the test box with a Faraday cage which could significantly decrease the amplitude of external electromagnetic fields inside the test box. A cage-like structure should be preferred over a fully closed metal box because the latter would prohibit the observation of discharges during the test. This would be a low-cost and low-effort solution that could bring fundamental change. Nevertheless, this method might have its limitations, as electromagnetic noise is not expected to alter the mean value of a signal.

**Gas supply.** Two minor observations concerning the nitrogen gas supply of the test box are proposed to a further investigation: First, the test box is designed to achieve an environment low in humidity and oxygen, in order to achieve the best and safest measurement results possible. Due to the construction of the test box, however, there is not a direct path for the nitrogen to replace the air underneath the GEM foil; the air can only slowly diffuse through the GEM holes. By determining the speed of this diffusion and examining if the humid air underneath the foil has an impact on the measurement, new insights could be gained. A quick fix can be the installation of small spacers between test box and drawer. Secondly, the gas influx is not measured or prescribed at GSI's test

---

<sup>22</sup>The airport Frankfurt is as near as 15 km; the HV path has on its longer side a length of around 75 cm, a quarter of the wavelength of air traffic control radio at approximately 120 MHz, but it is hard to estimate the significance of that.

setup. This has never been considered an issue as the hygrometers indicate when the environmental conditions are appropriate, independent on the influx. Yet, it was noticed that a gas influx above a certain threshold causes a vibration of the GEM foil which in turn visibly increases the fluctuation of the leakage current during the measurement. This should in theory just change the standard deviation of the leakage currents and not the mean value. Nevertheless, the examination of this effect can clarify its significance.

A final suggestion for an improvement of the leakage current test concludes this thesis. It has been explained in Chapter 4.1 that one of the most crucial points in the leakage current measurement is the offset taking. When the current measurement values are not corrected for the precise offset value, the deducted mean value loses its significance. During the course of this thesis, it was observed that this happens more often than one might expect. Besides, the GSI is one of the few institutes that provides the possibility to trace later on if the offset was correctly taken by including the seconds before and after offset taking in their measurement file. This is one reason for a lack of comparability between the institutes, because it cannot always be verified that the offset was correctly taken. Small adjustments can bring a big improvement in data quality: By prescribing that all institutes include the offset measurement in their measurement, it can be traced later on; this is a low-effort way to improve the reliability of the leakage current test.

## References

- [1] A. Andronic. An overview of the experimental study of quark-gluon matter in high-energy nucleus-nucleus collisions. *Int. J. Mod. Phys.*, A29, 2014.
- [2] P. Braun-Munzinger and J. Stachel. The quest for the quark-gluon plasma. *Nature*, 448(7151):302–309, July 2007. 10.1038/nature06080.
- [3] B. Abelev et al. Upgrade of the ALICE Time Projection Chamber. Technical Report CERN-LHCC-2013-020. ALICE-TDR-016, Oct 2013.
- [4] B. Abelev et al. Performance of the ALICE Experiment at the CERN LHC. *Int. J. Mod. Phys.*, A29:1430044, 2014.
- [5] F. V. Boehmer et al. Simulation of space-charge effects in an ungated GEM-based TPC. *Nuclear Instruments and Methods in Physics Research Section A: Accelerators, Spectrometers, Detectors and Associated Equipment*, 719:101–108, 2013.
- [6] G. Dellacasa et al. ALICE: Technical design report of the time projection chamber. 2000.
- [7] K. Aamodt et al. The ALICE experiment at the CERN LHC. *JINST*, 3, 2008.
- [8] P. Gasik. Building a large-area GEM-based readout chamber for the upgrade of the ALICE TPC. *Nucl. Instrum. Meth.*, A845:222–225, 2017.
- [9] F. Sauli. Principles of operation of multiwire proportional and drift chambers. 1977.
- [10] F. Sauli. *Gaseous radiation detectors: fundamentals and applications*. Cambridge monographs on particle physics, nuclear physics and cosmology. Cambridge Univ. Press, Cambridge, 2014.
- [11] F. Sauli. The gas electron multiplier (GEM): Operating principles and applications. *Nuclear Instruments and Methods in Physics Research Section A: Accelerators, Spectrometers, Detectors and Associated Equipment*, 805, 2016.
- [12] J. Wiechula. *Commissioning and calibration of the ALICE-TPC*. PhD thesis, University Frankfurt am Main, 2009.

## Acknowledgement

First and foremost, I would like to thank PD Silvia Masciocchi for giving me the opportunity to join the ALICE group at GSI, for her patient supervision and her multifaceted feedback. I further express my gratitude to Dariusz Miskowiec for his thorough explanations in the lab and helpful pieces of advice for my work. I would like to thank everyone in the group for being welcoming and assisting from the start.

I am indebted to all my friends and colleagues that helped with writing and provided mental support: First of all Mar Viñallonga, for her endless support from the other side of the globe. Julius Mildenerger, for clever ideas and keeping me in good mood. Martin Stein, for helpful critics and distractions from work. Thomas Rudzki, for good comments and many shared drives. Alexandra Datz, for her fast and good review.

# Erklärung

Ich versichere, dass ich diese Arbeit selbstständig verfasst und keine anderen als die angegebenen Quellen und Hilfsmittel benutzt habe.

Manuel Jahn

Heidelberg, den 7. März 2017